Environment International 130 (2019) 104748

Contents lists available at ScienceDirect

Environment International

journal homepage: www.elsevier.com/locate/envint

Review article

Nanomaterials-based treatment options for chromium in aqueous environments

Hubdar Ali Maitlo[a,1], Ki-Hyun Kim[a,*], Vanish Kumar[b,*], Sumin Kim[c], Jae-Woo Park[a]

[a] Department of Civil and Environmental Engineering, Hanyang University, 222 Wangsimni-ro, Seongdong-Gu, Seoul 04763, Republic of Korea
[b] National Agri-Food Biotechnology Institute (NABI), S.A.S. Nagar 140306, Punjab, India
[c] Department of Architecture and Architectural Engineering, Yonsei University, Seoul 03722, Republic of Korea

ARTICLE INFO

Handling Editor: Hefa Cheng

Keywords:
Cr(VI) removal
Adsorption
Electrocoagulation
Photoelectrocatalysis
Fuel cell
Performance evaluation

ABSTRACT

Sustainable development and the restoration of ecosystems are the important goals for civilization. Currently, heavy metal contamination of aquatic environments has become a serious issue. Chromium (Cr) is simultaneously an essential metallic element and one of 20 chemicals posing a maximum threat to living beings. To mitigate that threat, various treatment methods have been developed, including adsorption, electrocoagulation, photoelectrocatalysis, fuel cells, bioremediation, chemical precipitation, ultrafiltration, ion exchange, and co-precipitation. However, selection of the most energy- and cost-efficient wastewater treatment option has proven challenging, as each approach is subject to shortcomings involving energy consumption, treatment capacity, and efficiency. This review describes the potential role of diverse functional nanomaterials (e.g., iron/iron oxide nanoparticles, carbon nanostructures, metal organic frameworks, and their commercial counterparts) in treatment of Cr in aqueous environments with respect to key figure of merits, such as, adsorption capacity, removal efficiency, and partition coefficient. In addition, their performance was compared with the most common treatment options. The results of this study will help determine the most effective and economical options for control of Cr in aquatic environments.

1. Introduction

Environmental contaminants can easily propagate into the biosphere through various routes, including troposphere to exosphere, river to ocean, and natural to artificial ecosystem (Reddy and Cameselle, 2009). Human activities are considered indispensable components that can contaminate aquatic ecosystems (Pradhan et al., 2017). Contaminated water can deteriorate or damage the health not only of humans but entire ecosystems. According to US-Environmental Protection Agency (US-EPA), the presence of innumerable toxic contaminants such as oil spills (Kang et al., 2018; Li et al., 2018b; Sun et al., 2018; Zhang et al., 2018e; Zhang et al., 2019), organic dyes (Song et al., 2017; Zhang et al., 2017; Pan et al., 2018a; Pan et al., 2018b; Zhao et al., 2018a; Zhao et al., 2018b; Zhao et al., 2018c; Pan et al., 2019; Tian et al., 2019; Vu et al., 2019; Zhao et al., 2019), bacteria/viruses (Wang et al., 2018b; Zhang et al., 2018b; Yang et al., 2019), and heavy metals (Maitlo et al., 2019a; Vikrant and Kim, 2019; Vikrant et al., 2019) have aggravated ecosystem including water body. The prevailing capability of such contaminants is anticipated to be very high, depending upon the type of industrial activities (Aulakh et al., 2009; Schweitzer and Noblet, 2018; Mishra et al., 2019).

Among them, the non-biodegradable contaminants such as heavy metals (chromium) can enter and affect trophic chains without difficulty (Chansuvarn and Jainae, 2018). The chromium (Cr) is one of the most common metallic pollutants. It has been ranked one of the top 20 pollutants on the Superfund priority list of hazardous constituents for the past 15 years (Chrysochoou and Johnston, 2012). Anthropogenic sources of Cr include dyes (Ghosh et al., 2018), mining (Coetzee et al., 2018), electroplating (Wang et al., 2018a), automobile manufacturing (Rodríguez et al., 2018), metal processing (Lee et al., 2017), leather tanning (Angelucci et al., 2017), and textile manufacturing (Kuppusamy et al., 2017). Cr is dispersed throughout all types of environmental media, with chromite (+3) and chromate (+6) the most prevalent and stable forms (Pradhan et al., 2017). In groundwater, chromate approximately 1000 times as toxic as chromite and more mobile. (Keshmirizadeh et al., 2011). Cr(VI) is known as a group "A" anthropogenic carcinogen due to its mutagenic properties (Cieslak Golonka, 1996; Attia et al., 2010). As such, consumption of water

* Corresponding authors.
E-mail addresses: kkim61@hanyang.ac.kr (K.-H. Kim), vanish.saini01@gmail.com (V. Kumar).
[1] Present address: Department of Energy & Environment Engineering, Dawood University of Engineering & Technology, M.A. Jinnah road, Karachi 74800, Pakistan.

https://doi.org/10.1016/j.envint.2019.04.020
Received 6 February 2019; Received in revised form 18 March 2019; Accepted 8 April 2019
Available online 25 June 2019

contaminated with chromium can cause severe health complications for humans, such as liver damage, pulmonary congestion, edema, skin irritation, and ulcer formation (Raji and Anirudhan, 1998; Attia et al., 2010; Dhal et al., 2013).

In light of the severe toxicity of chromium, the US Environmental Protection Agency (EPA) has set a maximum guidance level of 100 μg L^{-1} for chromium discharged to inland surface waters (Heffron et al., 2016; Shahid et al., 2017). To meet environmental regulations, the effluent of wastewater containing chromium should be treated properly (Ali and Kim, 2018; Asri et al., 2018). Numerous treatment methods have been developed to tackle the issues caused by water and wastewater contaminated with chromium (refer to Section 4 for more details). However, most of the established treatment options are incapable of efficiently reducing chromium concentrations to permissible levels (Kobielska et al., 2018; Zare et al., 2018). Additionally, most conventional treatment systems require secondary treatments before discharging effluents (Shakya et al., 2018), making the process uneconomical.

Development of energy- and cost-efficient treatment options that address a variety of shortcomings (e.g., energy consumption, treatment capacity, operation cost/time, intensive operation, and less efficiency) has met with numerous obstacles (Kobielska et al., 2018; Maitlo et al., 2019a; Vikrant and Kim, 2019). To resolve these technical limitations, diverse forms of nanomaterials (NMs) with advanced functionalities and properties (e.g., high specific surface, short passage for diffusion, and tunable surface active sites) have been developed and applied to the sorptive removal of Cr (Wang et al., 2016b; Wang et al., 2016c; Arain et al., 2018; Kobielska et al., 2018; Wu et al., 2019). However, an appropriate sorbent material for treatment of Cr in water is proving elusive (Jiang et al., 2018).

This review evaluates the most effective nanomaterials for the sorptive removal of Cr from water. Diverse nanomaterials (e.g., iron/iron oxide, carbon, graphene/graphene oxide, metal organic frameworks, and their commercial counterparts) were studied. The most important operative parameters of the aforementioned nanomaterials were adsorption capacity, removal efficiency, and distribution coefficient. Each was evaluated as a key figure of merit against Cr ion removal. This work incorporates recent advances and describes existing obstructions and complications associated with nanotechnology. The performance of commonplace or conventional treatment options for Cr ions such as adsorption and photoelectrocatalysis (PEC) was also summarized for comparative purposes. We conducted in-depth performance evaluations of novel NMs as a means to expand their potential applicability to the remediation of Cr in aqueous environments. The results of this study will help determine the most effective and economical nanotechnology options to address Cr contamination.

2. Chromium sources, application, and its speciation in different types of water

Significant quantities of Cr are consumed globally each year by industrial and agricultural activities. Cr mining activities have multiplied considerably since early 1950s. According to the US Geological Survey (USGS), annual worldwide Cr production in 2017 amounted to 30.68 Gg, an increase of approximately 10% from five years previously (USGS, 2018) (Fig. 1). The major source countries of Cr in terms of mining activities were South Africa, Kazakhstan, India, and Turkey (Lukina et al., 2016; USGS, 2018). Approximately 95% of the world's Cr resources are found in South Africa and Kazakhstan (USGS, 2018), and these two countries have been considered the foremost producers of chromite ore (Shahid et al., 2017). Growing demand for Cr from various types of industrial activities (see Section 1 for more details) has considerably increased the cost of Cr (USGS, 2018) (Fig. 2).

Cr pollution is ubiquitous in the environment. It occurs in numerous oxidation states (from −2 to +6) according to the medium's chemical and physical properties (Malaviya and Singh, 2016). In aquatic environments, the predominant forms of chromium are inorganic species, which occur as oxyanions of hexavalent chromite and trivalent chromite (Pradhan et al., 2017). The coexistence of Cr(VI) ions with peroxo species typically leads to the formation of coordination complexes (Jin et al., 2016). However, Cr(III) remains relatively stable in acidic media and is more likely to be oxidized to chromate in alkaline media. Chromite can also form several types of octahedral coordination complexes (Pradhan et al., 2017). A speciation profile is therefore important component of chromium's redox chemistry. This profile is used for the proper identification as well as clarification of the chemical behavior of ionic species of Cr ions in aqueous media (Aroua et al., 2007; Shahid et al., 2017). Visual Minteq software was used to produce speciation profiles of aqueous Cr species that are present in diverse pH ranges (e.g., 1 to 14) at 25 °C (Fig. 3).

The extent of protonation depends on the pH of a solution. In oxygenated water, chromate exists predominantly as chromic acid (H_2CrO_4) at very acidic pH values (e.g., < 1). Likewise, in a pH range of 1–6, Cr would be available in the form of hydrochromate ($HCrO_4^-$), chromite hydroxide ($Cr(OH)^{2+}$), and chromite ions (Cr^{3+}). Similarly, at a pH higher than 8 (alkaline medium), chromate (CrO_4^{2-}) species exist predominantly as Cr(VI). In contrast, chromite (III) forms various types of ionic species in alkaline media (pH 8–12). More specifically, in a pH range of 8–10, chromite may occur preferably in the form of neutral species $Cr(OH)_3$. $Cr(OH)_4^-$ is prevalent only at extremely alkaline pHs (e.g., > 12).

3. Removal technologies for chromium in aqueous environments

Cr contamination in water deteriorates or damages the health of not only humans but also entire ecosystems. To date, several remediation procedures have been established. While chromium removal can involve complex mechanisms, it can be categorized into: direct adsorption of aqueous Cr(VI) (in the case of NMs); photocatalytic and cathodic reduction of Cr(VI) to Cr(III) (in the case of photocatalysis and fuel cells) (Gupta et al., 2001; Mohan and Pittman Jr, 2006; Kumar et al., 2007); chemical precipitation (Peters et al., 1985; Wang and Li, 2004; Sun et al., 2006); biological degradation (Laxman and More, 2002; Poornima et al., 2010), ion exchange (Rengaraj et al., 2001; Li et al., 2017); solvent extraction (Bentchikou et al., 2017), ultrafiltration (Haktanır et al., 2017; Muthumareeswaran et al., 2017); and photoelectrocatalysis (PEC) (Athanasekou et al., 2017; Chen et al., 2017; Sane et al., 2018).

Various types of fuel cells have also been introduced, including microbial (Li et al., 2018a; Wang et al., 2018c), microbial reverse-electrodialysis (Scialdone et al., 2014; D'Angelo et al., 2015), alkaline (Zhang et al., 2013), urine/Cr(VI) (Xu et al., 2016), iron-air fuel cell electrocoagulation (Maitlo et al., 2019c), and electrocoagulation (Aoudj et al., 2017; Un et al., 2017) (Fig. 4). However, most conventional methods suffer from technological and economic obstacles, such as high operative/processing costs, energy-expensiveness, excessive chemical consumption, and the generation of large quantities of hazardous secondary pollutants (Kumar et al., 2017; Vellingiri et al., 2017; Maitlo et al., 2019a). Most established systems are therefore unprofitable as large-scale control techniques for removal of Cr in aqueous systems (Kobielska et al., 2018; Jin et al., 2019). In an effort to upgrade removal efficiency, considerable research efforts have been devoted in recent years to the synthesis of novel nanomaterials that can effectively remove Cr from water, predominantly via adsorption (Samuel et al., 2019; Vikrant and Kim, 2019). The main objective of those technologies is to maximize Cr removal efficiency using chemically stable, energy-effective, and recyclable nanomaterials with reduced operating and processing costs.

4. Nanotechnology for the treatment of chromium

An ideal technology for remediation of harmful pollutants will be

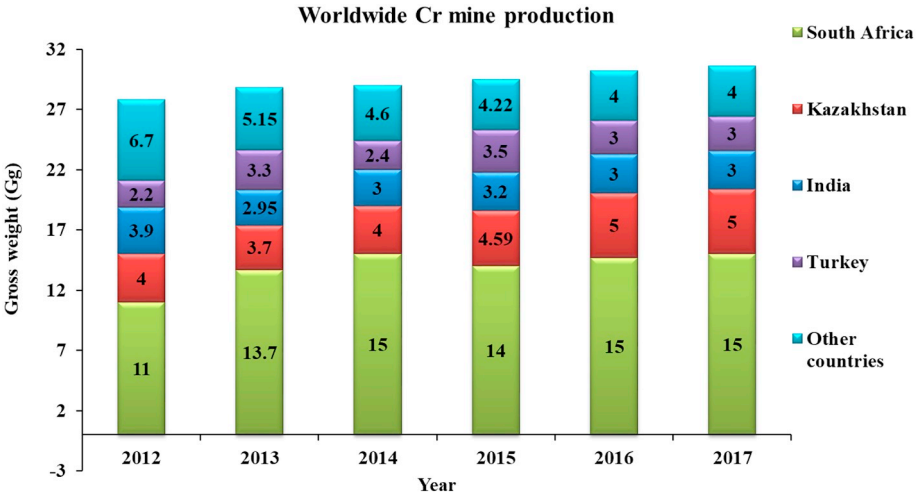

Fig. 1. Annual worldwide Cr mine production (USGS, 2018).

proficient, energy-efficient, and inexpensive to operate. In this regard, nanotechnology has been considered a leading contender (Kukkar et al., 2018). An exponential evolution has been observed in nanomaterial-based technologies in the 21st century (Kumar et al., 2017; Vellingiri et al., 2017; Vikrant and Kim, 2019). Numerous types of functional NMs (e.g., iron/iron oxide, carbon, titanium/titanium oxide, graphene/graphene oxide, and MOFs) imparted with a variety of physical and chemical properties (e.g., high water/chemical stability, large surface area, high porosity, strong binding affinity, unique electrical properties, and lighter density) have been developed as protective means to control Cr pollution in water (Table 1) (Arain et al., 2018; Burakov et al., 2018; Feng et al., 2018).

Various types of advanced NMs have been developed for the sorptive removal of aqueous heavy metal ions (Arain et al., 2018; Burakov et al., 2018; Feng et al., 2018). According to a literature review, adsorption capacity ($mg{\cdot}g^{-1}$) is the most commonly adopted parameter for appraising sorptive removal performance of NMs (Kraus et al., 2018; Le-Minh et al., 2018; Nigar et al., 2018). However, adsorption capacity can change through an interplay between the initial loading concentration (C_{in}) of the adsorbate (contaminants) and mass of the adsorbent (NMs) used in a sorption system. Therefore, the use of a distribution coefficient (Kp, in $mg\,g^{-1}\,\mu M^{-1}$) has been recommended as an alternative metric. Kp can be defined as the sorption capacity divided by the final concentration of sorbate remaining at an equilibrium (or maximal) adsorptive condition (Tran et al., 2016). Such a metric can be used to meaningfully evaluate the performance of NMs by balancing the effect of controlling factors such as an adsorbate/adsorbent as perceived for the partitioning of compounds between aqueous phases at equilibrium, i.e., Henry's law (Leo et al., 1971). In this regard, Kp has been a useful performance metric for NMs (in terms of heterogeneity of surface and strength of adsorption process) in place of adsorption capacity, and can be easily manipulated to yield expected values (Szulejko et al., 2018; Khan et al., 2019; Vikrant and Kim, 2019). Accordingly, we estimated maximum Kp values based upon our compilation of data for all NMs (Table 1).

4.1. Iron-based nanomaterials

Iron-based NMs have been gaining traction in wastewater treatment due to their advanced properties (high adsorption capacity, huge surface area-to-volume ratio, remarkable magnetic properties, robust biocompatibility, cost-effectiveness, and reusability) (Jain et al., 2018). However, surface insulation (passivation) and agglomeration are prerequisites for the expansion of the practical application of nanoscale zero-valent iron (nZVI)-based NMs (Ren et al., 2018). In the presence of atmospheric oxygen, the formation of a protective (passive) layer at the surface of bare nZVI would decrease the reactivity of nZVI NMs significantly (Zhu et al., 2018). As a result, various synthetic procedures (e.g., acid washing, hydrogen-reducing pretreatment, and application of ultrasonic energy) have been proposed as alternative approaches to

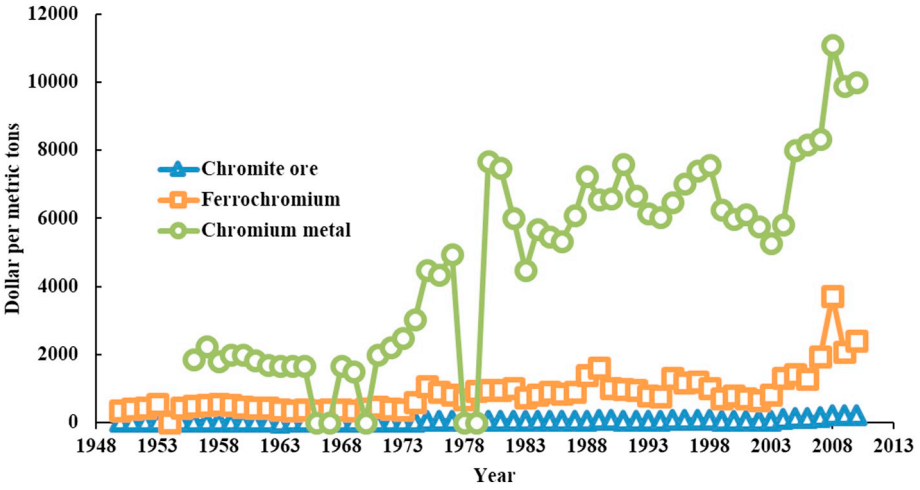

Fig. 2. Annual changes in Cr price (USGS, 2018).

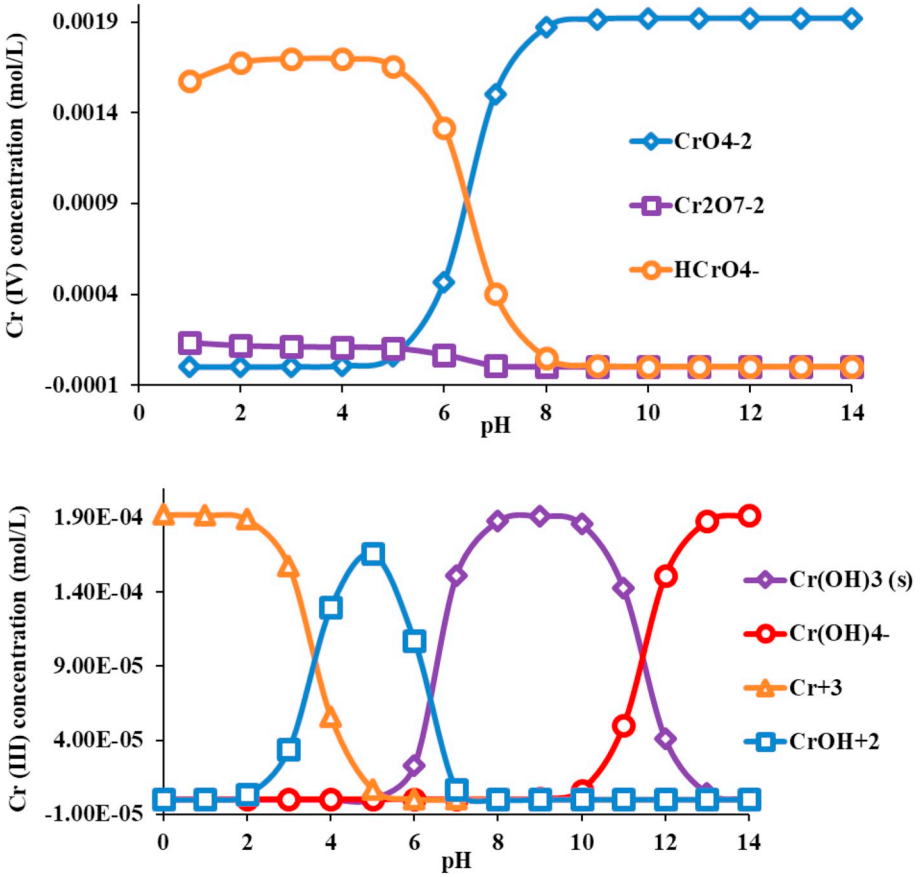

Fig. 3. Speciation profile of Cr in water with diverse pH range at 25 °C.

Fig. 4. Flow chart of various options available for the removal of chromium in water.

improving the reactivity of nZVI NMs for sorptive removal of Cr (Liou et al., 2005; Lai and Lo, 2008; Zhou et al., 2015). However, conventional synthesis methods suffer from technological and economic drawbacks, including high temperatures, excessive energy consumption, and deterioration of the crystalline structure of ZVI NMs (Zhang et al., 2018c). Consequently, liquid phase reduction was proposed as a new synthesis method for nZVI. Using this method, nZVI (iron nuclei of Fe^0) can be generated when the precursor of ferrous ions Fe(II) ($FeSO_4{\cdot}7H_2O$) are reduced by KBH_4 under nitrogen purging, shown as the reaction below (Zhang et al., 2018c).

$$Fe^{2+} + 2BH_4^- + 6H_2O \rightarrow Fe^0 \downarrow + 2B(OH)_3 + 7H_2\uparrow \quad (1)$$

The nZVI prepared by this method was found to hinder the formation of a passive layer, i.e., one formed due to oxides and hydroxides (or oxyhydroxides) of chromium and iron on its surface. Likewise, the use of graphene oxide (GO) as a skeletal support for Fe^0 was found to minimize passivation and aggregation of nZVI (Ren et al., 2018). We estimated maximum Kp values based upon our compilation of data for all iron-based NMs. According to the evaluation (Table 1), the as-prepared nZVI NMs exhibited superior performance compared with maghemite and magnetite, achieving a maximum Kp of 1073 mg g^{-1} μM^{-1} for the sorptive removal of Cr in water (Zhang et al., 2018c). The Kp values for maghemite and magnetite were calculated as 2.3 and 7.5 mg g^{-1} μM^{-1}, respectively (Jiang et al., 2013; Jain et al., 2018).

The Cr-removal performance demonstrated by nZVI NMs may be attributable to the presence of large numbers of surface active sites, high surface area (e.g., 182.97 m^2/g) (Table 2), and the rapid transfer of electrons from nZVI/$FeCr_2O_4$ to Cr(VI). Based on X-ray photoelectron spectrometer (XPS) analysis, we proposed a three-step mechanism for nZVI-based removal of Cr: (1) adsorption, (2) reduction, and (3) co-precipitation. The positively charged nZVI surface and its high surface area favor the adsorption of Cr(VI). The adsorption process was followed by the reduction of Cr(VI) to Cr(III). The interaction between Fe^0 and Cr(VI) was largely responsible for the reduction of Cr(VI). On nZVI

Table 1
Performance comparison of various nanomaterials for the adsorptive removal of Cr in water.

Order	Nanomaterial	Optimum adsorption condition (Temperature (°C, pH))	Initial Cr concentration (μM)	Maximum removal efficiency (%)	Maximum adsorption capacity ($mg\,g^{-1}$)	Final Cr concentration (μM)	Distribution coefficient ($mg\,g^{-1}$·μM)	Reference
[A] Iron/iron oxide–based nanomaterials								
1	Magnetite (Fe_3O_4)	25, 2	962	58.5	5.5	399	0.01	(Jain et al., 2018)
2	Magnetite (Fe_3O_4)	25, –	192	99	14.5	1.9	7.5	(Ren et al., 2017)
3	Maghemite (γ -Fe_2O_3)	26, 5	9.6	92.8	1.55	0.7	2.3	(Jiang et al., 2013)
4	rGO-nZVI	25, 3	769	99	50	7.7	6.5	(Ren et al., 2018)
5	EG-ZVI	20, 5.5	962	98.8	49.4	11.5	4.3	(Xu et al., 2018)
6	Fe_3O_4/AC	25, 2	962	95.3	8.1	45.2	0.2	(Jain et al., 2018)
7	Ppy-PANI/Fe_3O_4	25, 2	1923	99	303	19.2	15.6	(Kera et al., 2017)
8	NIOC	20, 5	71	90	69.8	7.2	9.81	(Lu et al., 2017a)
9	MNP/MWCNTs	25, 2	96.2	95	5	4.8	1.4	(Lu et al., 2017b)
10	nZVI	25, 3	1154	99.99	123.9	0.115	1073	(Zhang et al., 2018c)
11	GT-nZVI/Cu	30, 5	96.2	94.7	12.5	5.1	2.5	(Zhu et al., 2018)
12	MPC	–, 5	192	81.8	8.18	35.0	0.23	(Wen et al., 2017)
13	MCM-41	20, 5.7	962	19.5	19.5	774	0.03	(Chen et al., 2018)
14	nZVI	20, 5.7	962	61.3	65.3	372	0.18	(Chen et al., 2018)
15	nZVI/MCM	20, 5.7	962	94.2	97.7	55.8	1.75	(Chen et al., 2018)
16	LDHs	25, 5	577	29.7	24	406	0.06	(Wang et al., 2017b)
17	LDHs@MoS_2	25, 5	577	50.6	47	285	0.16	(Wang et al., 2017b)
[B] Carbon-based nanomaterials								
1	SWCNTs	25, 2.5	3.85	95	2.53	0.19	13.2	(Dehghani et al., 2015)
2	MWCNTs	25, 6	1.9	98	–	0.04	–	(Pillay et al., 2009)
3	MWCNTs	25, 2.5	3.85	75	1.26	0.96	1.3	(Dehghani et al., 2015)
4	MWCNTs	25, 6	385	60	–	154	–	(Gupta et al., 2011)
5	MCM-1	24.9, 3	1539	–	165	–	–	(Zhou et al., 2016)
6	MCM-1-Fe_3O_4	24.9, 3	1539	–	156	–	–	(Zhou et al., 2016)
7	s-MCM-41-NH_2	25, 2	2501	50.8	86.4	1230	0.07	(Fellenz et al., 2017)
8	I-MCM-41-NH_2	25, 2	2501	37.7	63.7	1558	0.04	(Fellenz et al., 2017)
9	CMM	25, 2	962	99	11.4	9.7	1.2	(Salam, 2017)
10	MCM-41-NH_2	25, 2	769	97	87.5	23.1	3.8	(Martin et al., 2017)
11	MnO_2/Fe_3O_4/ MWCNTs	61.9, 2	5770	–	187	–	–	(Luo et al., 2013)
12	PPy/OMWCNTs	25, 2	6732	99.99	294	0.67	437	(Bhaumik et al., 2016)
13	Magnetic-MWCNTs (MM)	25, 3	481	99.9	11.4	0.48	23.7	(Huang et al., 2015)
14	MWCNTs/nano-Iron	25, 6	384.7	90	–	38.5	–	(Gupta et al., 2011)
15	F-MC	25, 1	19,235	99.99	1423	1.92	740	(Cao et al., 2017)
16	NMC-100	25, 1	19,235	99.99	2001	1.92	1040	(Cao et al., 2016)
17	C@La-TiO_2	25, 5	577	41.8	8.2	336	0.02	(Wang et al., 2017a)
18	C@Ce-TiO_2	25, 5	577	36.5	7.2	366	0.02	(Wang et al., 2017a)
19	UMC	–, 3	19,234	99.99	203	1.92	106	(Gong et al., 2018)
18	MCPs-40	25, 1	2693	20	12.5	2154	0.01	(Huang et al., 2017)
19	MCFs-40	25, 1	2693	60	32.5	1077	0.03	(Huang et al., 2017)
20	FN-MC-66	–, 7	6155	99.99	97	0.62	157.6	(Huang et al., 2018)
[C] Graphene/graphene oxide based nanomaterials								
1	G	25, 2	269	–	87.1	–	–	(Yao et al., 2014)
2	GO	25,3	3847	66.2	49	1300	0.04	(Shaban et al., 2018)
3	GA	25,2	2885	–	122.3	–	–	(Liang et al., 2018)
4	GF	25, –	269	–	18.6	–	–	(Yao et al., 2014)
5	GFP	25, 2	269	–	348	–	–	(Yao et al., 2014)
6	Ppy-Fe_3O_4/rGO	44.85, 3	4328	–	293	–	–	(Wang et al., 2015)
7	RGO/NiO	25, 4	1924	91	198	173	1.14	(Zhang et al., 2018a)
8	AS-GO	54.85, 2	2308	–	215	–	–	(He et al., 2017)
9	8-HQ-GO-Fe_3O_4	34.85, 6.55	19.2	95.8	11.9	0.8	14.6	(Sheikhmohammadi et al., 2017)
10	PmPD/rGO/NFO	25, 3	962	–	503	–	–	(Wang et al., 2017c)
11	GS-Ppy	24.9, 2	1923	–	429	–	–	(Fang et al., 2018a)
12	Ppy-GO-NC	25, 2	3847	99.98	625	1	812	(Setshedi et al., 2015)
13	PmPD/rGO-0.1%	30, 1	15,003	–	526	–	–	(Jin et al., 2019)
14	GO-FH bio-nanocomposite	25, 2	1924	97	213	57.7	3.7	(Samuel et al., 2018a)
15	CS-GO	27, 2	1924	90	104	192	0.54	(Samuel et al., 2019)
16	GO-CS@MOF [Zn (BDC)(DMF)]	25, 3	962	90	145	96	1.5	(Samuel et al., 2018b)
17	PGA	25, 2	2886	–	168	–	–	(Liang et al., 2018)
18	TGA	25, 2	4809	–	190	–	–	(Liang et al., 2018)
19	TPGA	25, 2	4809	–	408	–	–	(Liang et al., 2018)
20	GSC	40, 1.5	385	93	2859	27	106	(Dubey et al., 2015)

(*continued on next page*)

Table 1 (*continued*)

Order	Nanomaterial	Optimum adsorption condition (Temperature (°C, pH))	Initial Cr concentration (μM)	Maximum removal efficiency (%)	Maximum adsorption capacity ($mg\,g^{-1}$)	Final Cr concentration (μM)	Distribution coefficient ($mg\,g^{-1}$·μM)	Reference
[D] Metal-organic framework								
1	Cu-BTC	–, 7	385	99.9	48	0.08	125	(Maleki et al., 2015)
2	ZJU-101	–	5770	96	245	23.8	1.1	(Zhang et al., 2015)
3	TMU-30	24.85, 9	577	95	145	28.9	5	(Aboutorabi et al., 2016)
4	MIL-100(Fe)_HF	25, 4	7694	–	26	–	–	(Fang et al., 2018b)
5	MIL-100(Fe)_no			–	40	–	–	
6	MIL-100(Fe) _TMAOH			–	42	–	–	
7	MIL-100(Fe) _Na_2CO_3			–	45	–	–	
8	UiO-66	25, 3	962	83	36.4	164	0.22	(Wang et al., 2017d)
9	UiO-66-OH		962	45	18.5	529	0.03	
10	UiO-66-OH_2		962	95.5	59.2	43.3	1.4	
11	Chitosan-MOF	40, 2	481	–	93.6	–	–	(Wang et al., 2016a)
12	IL-MIL-100(Fe)	25, 2	1923	88	286	231	1.2	(Nasrollahpour and Moradi, 2017)
13	Ag-triazolate MOF	30, 6	962	–	37	–	–	(Li et al., 2017)
14	Co-CP	30, 2.5	1924	90	38.5	192	0.2	(Lupa et al., 2018)
15	Co-Gly		1924	80	43.5	385	0.11	
16	Co-VP		1924	96	49	77	0.64	
17	ZIF-67	–, 7	289	88	15.4	34.6	0.45	(Li et al., 2015)
[E] Commercial nanomaterials								
1	AC	25, 6	962	99.99	52.6	0.10	547	(Heydari et al., 2013)
2	PAC	25, 2	4809	99.99	140	0.48	291	(Anupam et al., 2011)
3	Rice husk-drive AC	25, 2	2885	91.2	27	254	0.11	(Mullick et al., 2018)
4	ZRC-AC	40, 2	1923	77.6	196	431	0.46	(Labied et al., 2018)
5	Z-0.8	20, 3.4	1923	98	38.9	38.5	1.01	(Guan et al., 2009)
6	Z-1.2				54.4	38.5	1.41	
7	Z-1.6				65	38.5	1.69	
8	Z-2.0				75.8	38.5	1.97	
9	Micelle-clay complex	25, 6	962	86.0	9.43	135	0.07	(Qurie et al., 2013)

surfaces, Fe^0 was converted into Fe^{2+}, which provided sufficient number of electrons to reduce Cr(VI). In the last step, the Fe^{2+} and reduced form of Cr(VI), i.e., Cr(III) (as an oxyanion, e.g., $Cr_2O_4^{2-}$), were co-precipitated to form $FeCr_2O_4$.

Additionally, the production of bimetallic NMs and synthesis of nZVI may improve the removal of Cr by adsorption. Plant extracts containing flavonoids and polyphenols (e.g., sorghum bran, green tea, pomegranate, vine, and eucalyptus leaves) could reduce both Fe(II) and Fe(III) ions, effectively inhibiting the formation of agglomerates (Machado et al., 2013; Rao et al., 2013). Recently, novel functionalized nZVI NMs were reported to exhibit enhanced Cr removal capacity. For sorptive remediation of Cr, nZVI was assembled on reduced graphene oxide (rGO), green synthesized copper (GT-Cu), and expanded graphite (EG) to yield NMs of rGO-nZVI, GT-nZVI/Cu, and EG-nZVI, respectively (Ren et al., 2018; Xu et al., 2018; Zhu et al., 2018). If the sorptive removal performance of Cr was evaluated in terms of adsorption capacity, the capacity values of rGO-nZVI and EG-ZVI were comparable at ~50 $mg\,g^{-1}$ (Ren et al., 2018). However, comparisons based on Kp confirm that the performance of rGO-nZVI (Kp = 6.5 $mg\,g^{-1}\,\mu M^{-1}$) is far superior to others, such as EG-ZVI (Kp = 4.3 $mg\,g^{-1}\,\mu M^{-1}$) (Table 1). The superior performance of EG-ZVI, when assessed in terms of adsorption capacity, reflects differences in the initial loading conditions of Cr: 961.7 μM (EG-ZVI) over 769.4 μM (rGO-nZVI). In the case of rGO-nZVI, Cr removal was achieved through two mechanisms: (1) reduction of Cr(VI) to Cr(III) by Fe^0/Fe(II) and (2) generation of Cr $(OH)_3$ precipitates from Cr(III) on rGO surfaces. Oxygen-containing functional groups of rGO readily adsorbed Cr(III), which led to the formation of $Cr(OH)_3$ precipitates. The adsorption of Cr(III) on rGO surfaces also minimized the chances of Cr capping/passivation on nZVI surfaces. Nonetheless, the performance of rGO-nZVI was comparatively poor compared with many other functionalized iron oxide NMs (Kera et al., 2017; Lu et al., 2017a) (Table 1).

Iron oxide in the form of pure magnetite (Fe_3O_4) and its composites have been observed to be superior NMs for the adsorptive removal of aqueous chromium (Kera et al., 2017; Ren et al., 2017; Jain et al., 2018) (Table 1). More specifically, functionalized NMs such as polypyrrole (PPy)-PANI/Fe_3O_4, NIOC, EG-ZVI, and rGO-nZVI, enhance sorptive removal capacities against aqueous Cr (Kera et al., 2017; Lu et al., 2017a; Ren et al., 2018; Xu et al., 2018) (Table 1). For example, pristine Fe_3O_4 NMs was moderately effective (Kp = 7.53 $mg\,g^{-1}\,\mu M^{-1}$) but its performance was relatively poor compared with that of many other functionalized transition metal oxide NMs (e.g., iron oxide impregnated in chitosan beads (NIOC) (Kp = 9.81 $mg\,g^{-1}\,\mu M^{-1}$) and PPy–polyaniline (PANI)/magnetite (Fe_3O_4) Ppy-PANI/Fe_3O_4 (Kp = 15.75 $mg\,g^{-1}\,\mu M^{-1}$) NMs) (Kera et al., 2017; Lu et al., 2017a; Ren et al., 2017) (Table 1). A novel PPy-PANI/Fe_3O_4 NM with a core-shell structure was also synthesized by in situ chemical oxidative polymerization of pyrrole (Py) and aniline (ANI) monomers in the presence of magnetite (Fe_3O_4), using $FeCl_3$ as an oxidizing agent. The resulting functional magnetic novel nanocomposite (PPy-PANI/Fe_3O_4) demonstrated exceptional sorptive removal performance of aqueous Cr (Kp = 15.75 $mg\,g^{-1}\,\mu M^{-1}$), which was attributed to the reduction capabilities of Ppy-PANI toward Cr(VI) at low pH, e.g., 2 (Kera et al., 2017) (Table 1). Moreover, due to the ferromagnetic character of Fe_3O_4, PPy-PANI/Fe_3O_4 can be easily recovered from solution after treatment by applying a magnetic field.

In another report, iron oxide NMs impregnated in chitosan beads (NIOC) has been proposed as an efficient tool for Cr remediation (Fig. 5) (Lu et al., 2017a). A novel granular NIOC NM was prepared using iron oxide and chitosan (without glutaraldehyde and acid), a facile synthesis process and a sol-gel technique. The NIOC displayed sufficient tendency for Cr sorption compared with other iron-based (e.g., Fe_3O_4/AC and MNP/MWCNTs) and transition metal oxide NMs

Table 2
Sorption properties of various nanomaterials for the adsorptive removal of Cr in water.

S. No	Nanomaterial	BET surface area (m^2/g)	Adsorption temperature (°C and pH)	Co-existing ions	C_{in} (mg/L)[a]	Qmax (mg g^{-1})[b]	Isotherm model[c]	R^{2d}	Kinetic model[e]	R^{2f}	Reference
1	nZVI	183.0	25 °C, 3	Zn^{2+}, Cu^{2+}, PO_4^{3-}, NO_3^-, SO_4^{2-}, and CO_3^{2-}	60	123.9	L	0.99	PSO	> 0.99	(Zhang et al., 2018c)
2	Ppy-PANI/Fe_3O_4	56.5	25 °C, 2	Zn^{2+}, Cu^{2+}, Ni^{2+}, Cl^-, CO_3^{2-}, and SO_4^{2-}	100	303	L	0.999	PSO	> 0.99	(Kera et al., 2017)
3	NIOC	–	20 °C, 5	CO_3^{2-}, SO_4^{2-}-, SiO_3^{2}-, and $PO_4$3-	3.7	69.8	F	0.949	PSO	> 0.99	(Lu et al., 2017a)
4	NMC-100	56.2	25 °C, 1	–	1000	2001	L	0.98	PSO	> 0.99	(Cao et al., 2016)
5	F-MC	273	25 °C, 1	–	1000	1423	L	0.94	PSO	> 0.99	(Cao et al., 2017)
6	PPy/OMWCNTs	34.1	25 °C, 2	Zn^{2+}, Cu^{2+}, Ni^{2+}, F^-, NO_3^-, SO_4^{2-}, and CO_3^{2-}	350	294	L	0.999	PSO	> 0.99	(Bhaumik et al., 2016)
7	MM	–	25 °C, 3	–	25	11.4	L	0.998	PSO	> 0.99	(Huang et al., 2015)
8	GSC	157	40 °C, 1.5	–	20	2859	L	0.991	PSO	0.98	(Dubey et al., 2015)
9	Ppy-GO-NC	59.9	25 °C, 2	Zn^{2+}, Cu^{2+}, Ni^{2+}, Co^{2+}, Cl^-, and NO_3^-	200	625	L	0.999	PSO	> 0.99	(Setshedi et al., 2015)
10	8-HQ-GO-Fe_3O_4	–	34.85 °C, 6.55	–	1	11.9	L	0.994	PSO	0.99	(Sheikhmohammadi et al., 2017)
11	Cu-BTC	279	, 7	–	20	48	L	0.989	PSO	> 0.99	(Maleki et al., 2015)
12	TMU-30	–	24.85 °C, 10	Na^+, K^+, Cu^{2+}, Cd^{2+}, MoO_4^{2-}, and WO_4^{2-}	30	145	L	0.999	PSO	> 0.99	(Aboutorabi et al., 2016)
13	IL-MIL-100(Fe)	1451	25 °C, 2	–	100	286	L	0.9998	PSO	> 0.99	(Nasrollahpour and Moradi, 2017)
14	UiO-66	1123	25 °C, 3	K^+, Mg^{2+}, Ca^{2+}, Cl^-, and SO_4^{2-}	50	36.4	L	0.993	PSO	> 0.99	(Wang et al., 2017d)
15	UiO-66-OH	800	25 °C, 3		50	18.5	L	0.997	PSO	> 0.99	
16	UiO-66-OH_2	421	25 °C, 3		50	59.2	L	0.997	PSO	> 0.99	
17	Co-CP	–	30 °C, 2.5	–	100	38.5	L	0.999	PSO	> 0.99	(Lupa et al., 2018)
18	Co-Gly	–	30 °C, 2.5	–	100	43.6	L	0.999	PSO	> 0.99	
19	Co-VP	–	30 °C, 2.5	–	100	49	L	0.9995	PSO	> 0.99	
20	AC	–	25 °C, 6	–	50	52.6	L	0.99	–	–	(Heydari et al., 2013)
21	PAC	–	25 °C, 2	–	250	140	L	0.963	PFO	0.99	(Anupam et al., 2011)

[a] Initial Cr concentration.
[b] Maximum adsorption capacity.
[c] Isotherm model: Langmuir (L), Freundlich (F).
[d] Correlation factor for the isotherm model.
[e] Kinetic model: pseudo-first-order (PFO), pseudo-second-order (PSO).
[f] Correlation factor for the kinetic model.

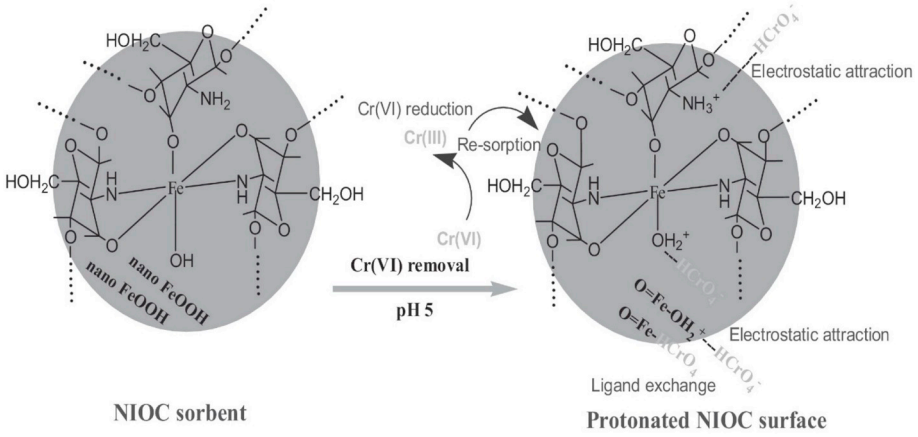

Fig. 5. Schematic of proposed Cr(VI) removal mechanisms on NIOC. Reproduced with permission from (Lu et al., 2017a).

(Kp = 9.81 mg g^{-1} μM^{-1}) (Lu et al., 2017a) (Table 1). The Cr removal mechanisms were attributed to electrostatic attraction and ligand exchange between protonated surface sites of NIOC (e.g., Fe-OH, Fe-OH^{2+} and NH^{3+}) and Cr metal ions as shown in the following reactions (Lu et al., 2017a) (2)–(4).

$$\text{Electrostatic attraction: } Fe - OH_2^+ + HCrO_4^- \rightarrow Fe - OH_2^+ \cdots HCrO_4^- \quad (2)$$

$$NH_3^+ + HCrO_4^- \rightarrow NH_3^+ \cdots HCrO_4^- \quad (3)$$

$$\text{Ligand exchange: } Fe - OH + HCrO_4^- \rightarrow Fe - HCrO_4 + OH^- \quad (4)$$

In many occasions, considerably high initial concentrations of aqueous Cr have been used to assess the adsorption capacity of NMs (e.g., Fe_3O_4, Fe_3O_4/AC, MCM-41, EG-ZVI, nZVI, and nZVI/MCM) (Chen et al., 2018; Jain et al., 2018; Xu et al., 2018). The sorption capacity values of aqueous Cr by Fe_3O_4, Fe_3O_4/AC, MCM-41, EG-ZVI, nZVI, and nZVI/MCM were estimated as 5.5, 8.1, 19.5, 49.4, 65.3, and 97.7 mg g^{-1}, respectively, at an initial concentration of 961.7 μM. However, if evaluated in terms of Kp (at a C_{in} of 961.7 μM), the values were not much impressive: 0.01, 0.2, 0.03, 4.28, 0.18, and 1.75 mg g^{-1} μM^{-1}, respectively. As such, Kp should be a more meaningful metric to assess the performance rather than adsorption capacity.

4.2. Carbon nanostructure–based Cr removal technologies

The synthesis of carbon nanotubes (SWCNTs), multi-walled carbon nanotubes (MWCNTs), and graphene-based materials and their composites has been the subject of considerable study, and they are widely known as attractive NMs for the sorptive removal of Cr (Herrero-Latorre et al., 2017). Carbon nanostructures possess advantageous mechanical, electric, optical, and magnetic properties for Cr adsorption (an extremely high aspect ratio; substantial surface area; small, hollow, and layered structures; chemical stability, a well-established mesoporous framework; π-π electrostatic interactions; light mass density; and strong binding energy) (Gupta et al., 2011; Dehghani et al., 2015; Bhaumik et al., 2016; Herrero-Latorre et al., 2017).

In a recent study, SWCNTs exhibited enhanced performance relative to MWCNT NMs for adsorptive removal of Cr. The distribution coefficient for Cr by SWCNT and MWCNT was 13.15 and 1.31 mg g^{-1} μM^{-1}, respectively, at a pH of 2.5 (Dehghani et al., 2015). These nanotubes exhibited both surface and pore adsorption for Cr. Moreover, SWCNTs favored more surface adsorption for Cr, when compared with MWCNTs. However, carbon-based NMs face their own significant technological and economic obstacles. Limits on the reusability of CNTs (due to very tiny size), for example, have been a severe limiting factor (Luo et al., 2013). Modifications of MWCNTs with Fe_3O_4-imparted magnetic characters in MWCNTs may prove helpful for easy and fast recovery of the NMs. Moreover, Fe_3O_4 exhibited electrostatic interactions with Cr (VI). Furthermore, modification of such systems with metal-ion scavengers, e.g., MnO_2, have led to enhanced Cr removal efficiencies of MWCNTs. At a pH of 2, the MWCNTs modified with Fe_3O_4 and MnO_2 (MnO_2/Fe_3O_4/MWCNTs) exhibited an adsorption capacity of 186 mg g^{-1} for Cr(VI) due to electrostatic interactions, cation exchange, and surface complexation mechanisms. (Note that both MnO_2 and Fe_3O_4 displayed electrostatic interactions with Cr(VI) at acidic pH values). Likewise, a chitosan (CS)-based gel was developed by modifying MWCNTs with poly(acrylic acid) and poly(4-amino diphenyl amine) to improve Cr sorptive removal and recyclability (Kim et al., 2015). As a result, CNT-based nanocomposites (e.g., magnetite/MWCNTs, chitin/magnetite/MWCNTs, and PPy/OMWCNTs NCs) have been proposed to ameliorate the adsorptive removal attributes of CNTs for Cr remediation (Sarkar et al., 2018).

Magnetite/MWCNTs (MM) and chitin/magnetite/MWCNTs (CMM) nanocompounds have also been produced. Here, magnetite and chitosan were mixed with the pure MWCNTs to enhance their magnetic and sorptive properties, respectively (Salam, 2017). According to the performance evaluation, the Kp values of MM (23.7 mg g^{-1} μM^{-1}) were far superior to that of CMM (1.2 mg g^{-1} μM^{-1}), although they exhibited an almost identical adsorption capacity (11.4 mg g^{-1}) (Table 1). Such disparities in Kp values could be due to the substantial difference in initial loading concentrations of the aqueous Cr (MM = 481 μM vs. CMM = 961.7 μM) and removal efficiency in their sorption processes. Accordingly, MMs appear to be superior sorptive media for the removal of aqueous chromium (Huang et al., 2015; Salam, 2017).

In addition, the use of PPy-wrapped oxidized multi-walled carbon nanotube (PPy/OMWCNT) NCs has been demonstrated to be an effective approach to aqueous Cr remediation (Bhaumik et al., 2016). PPy/OMWCNTs NCs synthesized with an in situ chemical oxidative polymerization method exhibited an exceptional tendency for Cr sorption (e.g., Kp of 436.7 mg g^{-1} μM^{-1}) (Bhaumik et al., 2016) (Table 1). The mechanism of Cr removal was attributed to the electrostatic attraction between protonated surface sites of PPy/OMWCNTs and Cr metal ions (Bhaumik et al., 2016).

Among the reported CNT-based NMs (e.g., SWCNTs, MWCNTs, MM, CMM, and PPy/OMWCNTs), novel magnetic carbons doped with nitrogen (NMC-100) and fluorine (F-MC) have shown high adsorptive potentials for Cr removal (Cao et al., 2016; Cao et al., 2017). Chemical oxidization of CNTs with doping by heteroatoms such as nitrogen, fluorine, and sulfur can accommodate a variety of structural defects (e.g., heptagons and pentagons) or vacancies pertaining to the hexagonal network of carbon (Li et al., 2013; Cai et al., 2014). In comparison, the electrochemical properties (e.g., chemical reactivity as well as negative charge density) of nitrogen-doped CNTs (NMC-100) should be significantly superior to those of pure CNTs (Zhang et al., 2014; Lin et al., 2016). Such an advancement in CNTs suggests the possibility of

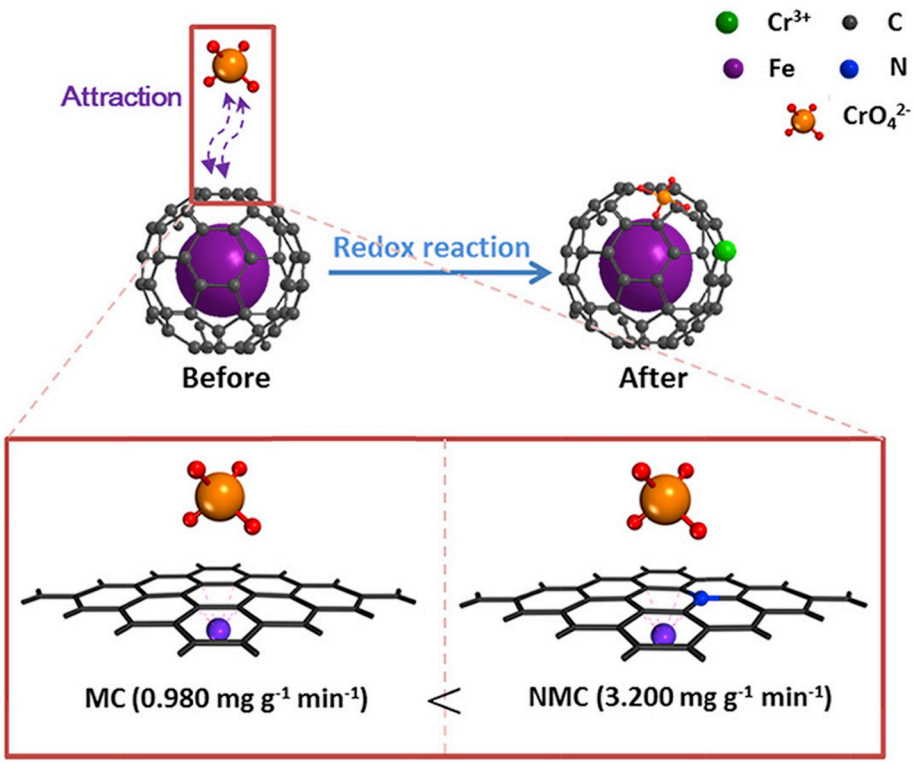

Fig. 6. Schematic of proposed Cr(VI) removal mechanisms on NMC-100. Reproduced with permission from (Cao et al., 2016).

significantly increased surface functionalities and reactive anchoring sites for Cr adsorption (Zhang et al., 2014; Cao et al., 2016; Lin et al., 2016).

Core-shell-structured magnetic carbons doped with nitrogen (NMC-100 with melamine as a precursor) as well as fluorine (F-MC with polyvinylidene fluoride as a precursor) were synthesized by an in situ chemical facile pyrolysis carbonization procedure. The nanocomposite (NMC: 1040.5 mg g^{-1} μM^{-1}) demonstrated superior sorptive removal of aqueous Cr compared with the latter (F-MC: 740 mg g^{-1} μM^{-1}) (Cao et al., 2016; Cao et al., 2017) (Table 1). The extraordinary sorptive performance of NMC-100 NMs toward Cr can be credited to the incorporation of nitrogen over magnetic nanocarbon. Such an effect is expected to enhance the charge density of NMs, improving the magnetic attraction between NMC-100 and Cr metal species (Cao et al., 2016) (Fig. 6). Similarly, magnetic carbons in various morphologies (fibrillar "MCFs" and particulate carbons "MCPs") or doped with hybrid mixture of fluorine and nitrogen (FN-MC-66) have been utilized for the sorptive removal of aqueous Cr (Huang et al., 2017; Huang et al., 2018). Accordingly, the FN-MC-66 composite exhibited far superior sorption potential (e.g., Kp of 157.6 mg g^{-1} μM^{-1}) against Cr over MCFs (0.01 mg g^{-1} μM^{-1}) or MCPs (0.03 mg g^{-1} μM^{-1}). The observed performance of FN-MC-66 was accounted for by the enhanced negative charge density of fluorine and nitrogen used for doping. More specifically, the graphitic N and heteroatoms at defects, edges, or vacancies should have provided the utmost imperative active sites for the FN-MC-66 to stimulate sorption of aqueous Cr (Huang et al., 2018).

Graphene is another carbon nanostructure that warrants consideration. Graphene has an two-dimensional hexagonal framework that exhibits favorable optical transparency, mechanical strength, and thermal/electrical conductivity, and it has become a preferred material for the treatment of heavy metals (Solís-Fernández et al., 2012; Peng et al., 2017). Bottom-up organic synthesis, mechanical exfoliation, chemical vapor deposition, unzipping of carbon nanotubes, ball milling of graphite, liquid-phase exfoliation, and reduction of graphene oxide have been applied to synthesize graphene NMs (Peng et al., 2017) (Fig. 7). The monolayer graphite oxide is known for its high hydrophilicity, hydrophobic π-π interaction, and superior surface charge density due to the existence of highly effective functional groups (hydroxyl and carboxylic acid) (Ramesha et al., 2011).

According to a recent literature review, many forms of graphene are available, including graphene oxide (GO), 3-aminopropyltriethoxysilane-functionalized graphene oxide (AS-GO), reduced graphene oxide/NiO (RGO/NiO), chitosan-grafted graphene oxide (CS-GO), and graphene oxide (GO)/chitosan (CS)/metal organic framework (GO-CS@MOF [Zn(BDC)(DMF)]). A performance evaluation with respect to adsorption capacity and Kp values found most of the tested graphene-based NMs are ineffective (e.g., they have a higher capacity but a lower Kp value) at sorptive removal of aqueous Cr (Table 1). High initial concentrations of aqueous Cr can explain the adsorption capacity of some of the graphene-based NMs (e.g., GO-CS@MOF [Zn(BDC)(DMF)], GO-FH-nanocomposite, and PPy-GO-NC). Sorption capacity values are often exaggerated with increased quantities of C_{in}. Ranking by sorption capacity produces the order: GO-CS@MOF [Zn(BDC)(DMF)] (145 mg g^{-1}) < GO-FH-nanocomposite (212.8 mg g^{-1}) < Ppy-GO-NC (625 mg g^{-1}) at C_{in} of 962, 1923.5, and 3847 μM, respectively. (Table 1). However, Kp values are more than two orders of magnitude lower 1.5, 3.7, and 812.4 mg g^{-1} μM^{-1}, respectively. The reason for the disparity between the two parameters again reflects the combined effect of the initial loading concentration of Cr and different efficiencies in sorption processes. GO-Fe_3O_4 functionalized with 8-hydroxyquinoline (8-HQ- GO- Fe_3O_4) was more proficient at sorptive removal of Cr (14.63 mg g^{-1} μM^{-1}) than other compounds (e.g., GO, CS-GO, and RGO/NiO) (Sheikhmohammadi et al., 2017) (Table 1).

When a simple chemical approach is used to synthesize novel graphene sand composite (GSC) with the application of a highly carbonaceous source (sucrose $C_{12}H_{22}O_{11}$), the composite exhibited a maximum Kp value of 106.2 mg g^{-1} μM^{-1} for Cr removal at a pH of 1.5 (Dubey et al., 2015) (Table 1). The GSC appeared to remove Cr through two mechanisms, direct and indirect reduction. In case of the former, the electron donor groups (e.g., –OH, C═O, and O-CH_3) present on the surface of the GSC led directly to the reduction of Cr(VI) to Cr(III). More specifically, an adsorption-induced reduction mechanism involving the

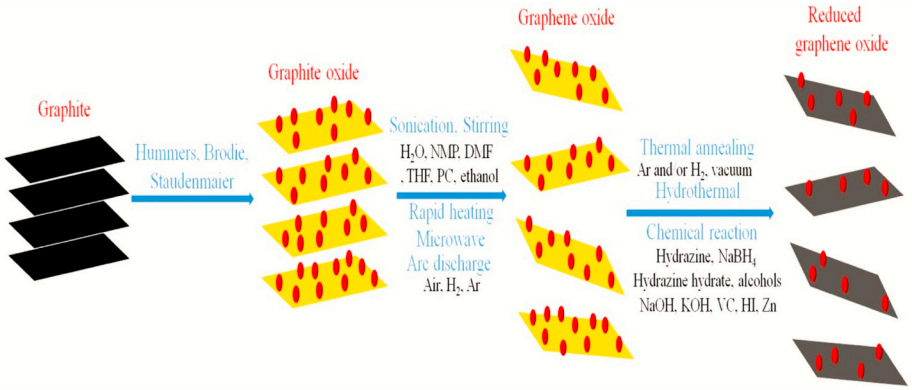

Fig. 7. Synthesis process of GO and rGO from the pristine graphite. Reproduced with permission from (Peng et al., 2017).

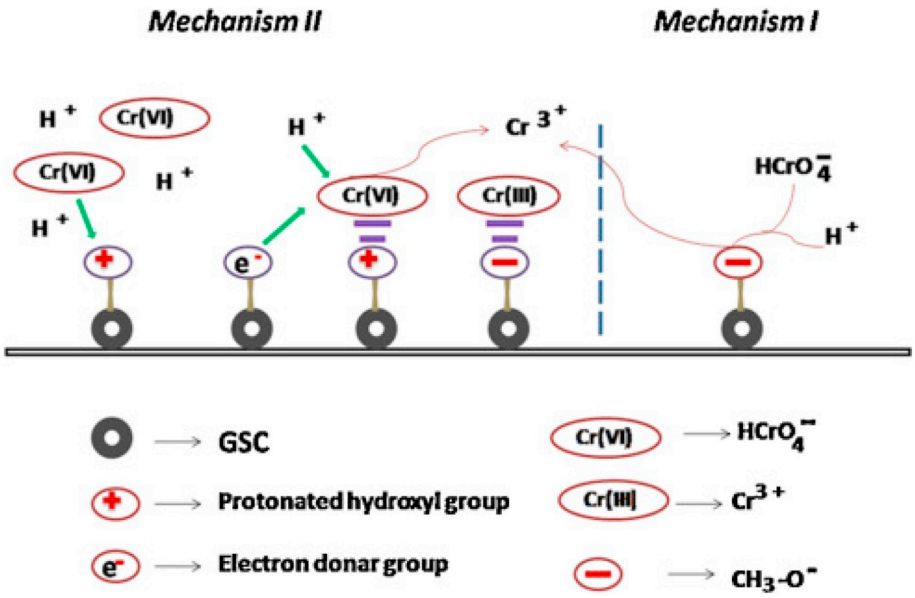

Fig. 8. Schematic diagram of proposed Cr(VI) removal mechanisms on GSC. Reproduced with permission from (Dubey et al., 2015).

conversion of Cr(VI) to Cr(III) has been proposed for the remediation of aqueous Cr through the application GSC NMs (Fig. 8). The removal mechanism for indirect reduction is expected to consist of three steps: (1) electrostatic attraction between protonated surface sites of GSC and chromate ions; (2) reduction of chromate to chromite by adjacent electron-donor functional groups (OH^-, C═O, O−CH_3) of the graphene sand; and (3) adsorption of reduced Cr(III) on the surface of GSC NMs through the formation of a coordinated covalent bond between the carbonyl (C═O)/methoxy groups (O−CH_3) and Cr(III) (Dubey et al., 2015).

As discussed in Section 4.2, the NMs containing pyrrole (e.g., PPy/OMWCNT: Kp of 436.7 mg g^{-1} μM^{-1}) and nitrogen (NMC: Kp of 1040.5 mg g^{-1} μM^{-1}) have demonstrated exceptional sorptive removal capacity for Cr in aqueous systems (Bhaumik et al., 2016; Cao et al., 2016) (Table 1). NMs modified with the nitrogen, fluorine, sulfur, and PPy can favorably accommodate multiple structural defects (e.g., heptagons and pentagons) or vacancies pertaining to the hexagonal network of the material (Li et al., 2013; Cai et al., 2014). Consequently, the electrochemical properties (e.g., chemical reactivity as well as negative charge density) of these NMs (e.g., NMC and PPy/OMWCNT) should be significantly superior to their pristine forms (Zhang et al., 2014; Bhaumik et al., 2016; Cao et al., 2016; Lin et al., 2016). Such an advancement in CNTs suggests the possibility of significantly increased surface functionalities and reactive anchoring sites for Cr adsorption (Zhang et al., 2014; Cao et al., 2016; Lin et al., 2016).

A similar approach has also been applied to GO to produce novel pyrrole (Py) and nitrogen-contained GO NMs. Recently, in situ chemical synthesis of PPy-GO nanocomposites (PPy-GO NCs) has been applied to Cr removal (Setshedi et al., 2015). A PPy-GO NC with a Kp value of 812.4 mg g^{-1} μM^{-1} has proven to be the most effective GO-based novel NM for the sorptive removal of Cr (Setshedi et al., 2015) (Table 1).

4.3. Metal-organic framework

The adsorption method is considered one of the most effective and simplest treatment options for the removal of heavy metals from aqueous media. Apart from the porous NMs described above, attention has been paid to inorganic-organic hybrid porous materials, known as metal-organic frameworks (MOFs) (Feng et al., 2018). To date, > 80,000 different categories of MOF-based NMs have been applied to a broad field of environmental applications (Espallargas and Coronado, 2018). Numerous synthesis methods (e.g., hydrothermal, conventional heating, sonochemical, solvothermal, layer-by-layer, microwave, mechanochemical, thin-film, and electrochemical) can produce MOF-based NMs (Feng et al., 2018).

Among the many MOFs and their modified forms that have been introduced to remove Cr are cobalt vinyl phosphonic acid (CO-VP), Zr-based MOFs of UiO-66 (UiO-66-OH_2), $(Pb(INO)_2)_2$·DMF (TMU-30), cationic Zr-MOF (ZJU-101), acidic chloroaluminate (IL)- and iron (Fe)-modified MIL-100 (IL-MIL-100[Fe]), and copper-

benzenetricarboxylate-based MOF (Cu-BTC) (Maleki et al., 2015; Zhang et al., 2015; Aboutorabi et al., 2016; Nasrollahpour and Moradi, 2017; Wang et al., 2017d) (Table 1). The performance of MOFs can be evaluated in terms of Kp value. Cu-BTC, at 124.8 mg g^{-1} μM^{-1}, for example, greatly outperformed UiO-66-NH_2 (1.4 mg g^{-1} μM^{-1}) or Co-VP (0.64 mg g^{-1} μM^{-1}). However, when all three were assessed in terms of adsorption capacity, little difference was observed (48 to 59.2 mg g^{-1}) (Table 1). Such disparities can be explained by the large difference in the initial loading concentration of Cr: Cu-BTC = 384.7, UiO-66-NH_2 = 961.7, and Co-VP = 1923.5 μM (Table 1). In comparison, (Pb$(INO)_2)_2$·DMF (TMU-30) reportedly exhibits enhanced selectivity for Cr over a wide pH range of 2 to 9, with a maximum Kp of 5 mg g^{-1} μM^{-1}. The relatively large Kp value of TMU-30 has been attributed to the stronger positive charge potential of pyridine carboxylate N-oxide derivatives (Aboutorabi et al., 2016) (Table 1). Likewise, Zr-MOF (ZJU-101), which contains NO_3^- and immobilized pyridyl N^+–CH_3 on its pore surface, has been shown to be an effective option for aqueous Cr remediation (Zhang et al., 2015). The novel compound ZJU-101 exhibited moderately high aqueous Cr sorption (e.g., Kp of 6.4 mg g^{-1} μM^{-1}) (Zhang et al., 2015) (Table 1). The superior selectivity for Cr sorption by ZJU-101 can be credited to the strong coulombic attraction between the framework (the positive ligand of ZJU-101) and negatively charged Cr ions ($Cr_2O_7^{2-}$) (Fig. 9).

Among the reported MOF-based NMs (e.g., CO-VP, UiO-66-OH_2, IL-MIL-100(Fe), TMU-30, and ZJU-101), the novel copper-benzenetricarboxylate-based MOF (Cu-BTC) NM has demonstrated a relatively high adsorptive potential for Cr removal (Table 1). Cu-BTC is known for its high surface area, accessible coordinative unsaturated sites, uniform pore size, and superb water/chemical stability (Maleki et al., 2015). The maximum Kp value of Cu-BTC for Cr ion ($Cr_2O_7^{2-}$) was found to be 124.8 mg g^{-1} μM^{-1} (Maleki et al., 2015) (Table 1). Its maximum Kp occurred at a neutral pH (pH 7).

4.4. Commercial materials for chromium removal

Numerous types of novel NMs have been assessed for their potential for sorptive removal of aqueous Cr due to their mechanical, electric, optical, and magnetic properties; extremely high aspect ratio; substantial surface area; small, hollow, layered structures; chemical stability; mesoporous framework; π-π electrostatic interactions; light mass density; functionalizing ligands; and strong binding energy (Dehghani et al., 2015; Bhaumik et al., 2016; Herrero-Latorre et al., 2017). On the other hand, some advanced NMs have shown operative limitations, such as high preparation costs, hydrolytic instability, reactivation after adsorption saturation, microscopically irreversible sorption, and selectivity challenges (Labied et al., 2018; Szulejko et al., 2018). In this context, much attention has been paid to commercially available materials such as activated carbon (AC), rice hulk-drive AC, *Ziziphus jujuba* rubidium carbonate–activated carbon (ZRC-AC), micelle-clay complexes, and zeolite (Z) (Table 1). According to performance evaluations with respect to Kp values, most of these commercial options are less effective in comparison with novel NMs, including micelle-clay complexes (0.07 mg g^{-1} μM^{-1}) (Qurie et al., 2013), rice hulk-drive AC (0.11 mg g^{-1} μM^{-1}) (Mullick et al., 2018), ZRC-AC (0.46 mg g^{-1} μM^{-1}) (Labied et al., 2018), and Z-0.8, Z-1.2, Z-1.6, and Z-2.0 (1.01, 1.41, 1.69, and 1.97 mg g^{-1} μM^{-1}) (Guan et al., 2009). Among the commercial products, pure AC has shown superior adsorptive potential for Cr removal due to its physiochemical properties. AC exhibits mesoporous and microporous characteristics with widespread variation in their proportion; reasonably high internal surface area and mechanical strength; and diverse functional groups (quinone, carbonyl, lactone, and phenol) (Anupam et al., 2011; Heydari et al., 2013; Burakov et al., 2018). The Kp value of AC was relatively high, ranging from of 291.1 to 546.9 mg g^{-1} μM^{-1} (Table 1). The maximum Kp value at an acidic pH (e.g., 2) can be attributed to the electrostatic attraction between protonated surface sites of AC and Cr metal ions (Karthikeyan et al., 2005; Anupam et al., 2011; Heydari et al., 2013).

5. Adsorption isotherm and kinetic studies of aqueous Cr removal by NMs

5.1. Adsorption isotherm model analysis

Mathematical adsorption isotherm models have been used to quantify classify sorptive removal mechanisms of contaminants from aquatic environments to a solid-phase at a constant temperature and pH

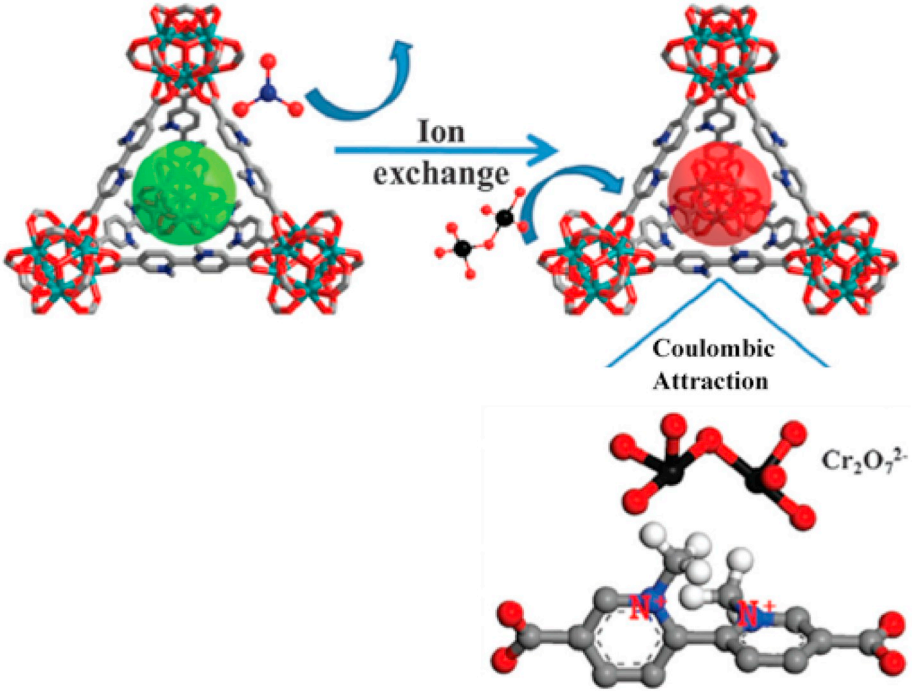

Fig. 9. Schematic of proposed Cr(VI) removal mechanisms on ZJU-101. Reproduced with permission from (Zhang et al., 2015).

(Vikrant et al., 2018). In addition, various types of isotherm models have been developed. Among them, the Langmuir and Freundlich models have been explored most extensively for the simulation of aqueous Cr sorption removal by NMs (Foo and Hameed, 2010; Samuel et al., 2018b).

$$\text{Langmuir: } Q_e = \frac{K_L Q_m C_e}{1 + K_L C_e} \quad (5)$$

$$\text{Freundlich: } Q_e = K_F C_e^{1/n} \quad (6)$$

where C_e (mg/ L) is the equilibrium concentration of the contaminant, while Q_e (mg g^{-1}) and Q_m (mg g^{-1}) are the equilibrium and theoretical isotherm saturation adsorption capacities, respectively. K_L and K_F represent the Langmuir bonding terms related to the interaction energies (L mg^{-1}) and the Freundlich affinity coefficient (L $mg^{-1})^{1/n}$, respectively. n refers to adsorption intensity.

The Langmuir isotherm model postulates the monolayer sorption of aqueous Cr ions over the fixed/definite sorptive sites of the NMs (Liang et al., 2018). It describes homogeneous sorption with constant enthalpies and activation energy (Foo and Hameed, 2010; Liang et al., 2018). In other words, it involves an equilibrium saturation point, or plateau, where more than one molecule cannot be adsorbed by a surface site of the NMs. In contrast, the Freundlich isotherm model has most frequently been used to typify the non-ideal multilayer sorption mechanism of aqueous Cr ions over the heterogeneous sorptive sites of NMs (Liang et al., 2018; Lupa et al., 2018). The Freundlich model exhibits non-uniform distribution of adsorption enthalpy over the heterogeneous surface; it increases with surface coverage of the NMs (Foo and Hameed, 2010; Liang et al., 2018). According to the isotherm model validation, the Langmuir isotherm was often the more suitable ($R^{2d} > 0.99$) model for the sorptive removal of aqueous Cr by diverse NMs (Table 2). The aqueous Cr ions would generate monolayer surface complexes with homogeneous surfaces of the NMs to occupy the available reactive sites (e.g., fixed/definite sorptive sites) of the NMs.

5.2. Kinetic model analysis

The large adsorption capacities of NMs for aqueous (or gaseous) pollutants could be due to interactive reactions (e.g., physisorption and chemisorption) between pollutants and ultramicropores or functional groups of the NMs (Puthiaraj et al., 2017; Feng et al., 2018). For physisorption, interactions between the adsorbate and the sorbent bed are controlled by weak van der Waals forces. In contrast, chemisorption can be associated with elevated amounts of surface functionalities that would help strengthen the interactions (e.g., hydrogen bonding, electrostatic interaction, and π–π stacking interaction) between anchoring sites of NMs and pollutants (e.g., Cr) (Lu et al., 2017a; Feng et al., 2018). Therefore, numerical (kinetic) models are preferable tools for exploring adsorptive Cr removal on advanced NMs (Zhou et al., 2016). The selection of a suitable kinetic model is the most important task for describing the conflicting effects of diverse operative factors (e.g., operating cost/time and experimental efforts) and optimization of the sorption process (Wang et al., 2017c). Pseudo-first-order (PFO) and pseudo-second-order (PSO) models have been used extensively to describe the Cr sorptive removal mechanism via advanced NMs, as expressed in Eqs. (7) and (8) (Cao et al., 2017; Wang et al., 2017c; Janik et al., 2018).

$$\text{PFO: } Q_t = Q_e(1 - e^{(-K_1 t)}) \quad (7)$$

$$\text{PSO: } Q_t = \frac{K_2 Q_e^2 t}{(1 + K_2 Q_e t)} \quad (8)$$

where K_1 (min^{-1}) and K_2 (g mg^{-1} min^{-1}) are the adsorption rate constants of PFO and PSO kinetic models, respectively. Q_t and Q_e represent the adsorbed amounts of pollutant at time t (min) and equilibrium, respectively.

The PFO kinetic model is commonly used to characterize the physisorption process, while the PSO kinetic model is generally used for chemisorption. The higher correlation coefficients (R^2) value suggests a more pertinent model for the kinetics of Cr adsorption. According to a literature review on Cr removal by NMs (Table 2), the experimental data can be better fit to the PSO kinetic model with higher R^{2f} values (e.g., $R^{2f} > 0.99$). Based on such evidence (Table 2), chemisorption appears to be the main mechanism for Cr removal using advanced NMs.

6. Performance evaluation of NMs for sorptive removal of aqueous Cr

An effective Cr sorptive material should perform well in water samples. To test the real-world applicability of Cr sorptive materials, the performance of a given material must be evaluated at varying experimental parameters, and the aforementioned NMs have been explored in varying experimental conditions, e.g., pH and co-ion presence, depending on data availability. In this section, the performance of NMs for the removal of Cr has also been compared in a respect to the broader category of adsorbents vs. catalysts.

6.1. Effects of pH on Cr removal

The pH of a testing solution is one of the critical factors that govern aqueous Cr sorption on an adsorbent surface (Kera et al., 2017; Zhang et al., 2018c). The nature of physicochemical interactions between heavy metal ions and sorption sites of NMs depends heavily on the pH of the solution used in adsorption methods (Cao et al., 2017; Lu et al., 2017a). Moreover, the suspension and stability of colloidal particles depend exclusively on their surface charge. If the particles possess different charges (e.g., a negatively charged adsorbate and a positive charged sorbent), they might attract each other and ultimately precipitate onto the surface of solid colloids (NMs) (Ghernaout et al., 2011; Maitlo et al., 2019a; Maitlo et al., 2019d). According to the Eh-pH (Pourbain) diagram, under acidic pH conditions (e.g., < 6), hydrochromate ($HCrO_4^-$) ions exist predominantly as the major Cr(VI) species in aqueous solutions (Fig. 3). Thus, at an acidic pH, a higher Cr sorptive removal efficiency could be attributed to the strong electrostatic attraction between negatively charged Cr ions (e.g., $HCrO_4^-$) and the positively charged surface of the NMs (e.g., nZVI, PPy-PANI/Fe_3O_4, PPy/OMWCNTs, and NMC-100). Subsequently, the optimal performance of the adsorption process for aqueous Cr removal was in a pH range of 2–3 (Tables 1–2).

6.2. Effects of co-existing ions

Most of the groundwater as well as industrial wastewater (e.g., from tanning, mining, and electroplating) contains a high concentration aqueous Cr(VI) ions along with other co-existing cations (e.g., Na^+, K^+, Mg^{2+}, Ca^{2+}, Zn^{2+}, Cu^{2+}, and Cd^{2+}) and anions (e.g., F^-, Cl^-, NO_3^-, SO_4^{2-}, and CO_3^{2-}, MoO_4^{2-}, WO_4^{2-}, and PO_4^{3-}) (Bhaumik et al., 2016; Kera et al., 2017; Maitlo et al., 2018a; Zhang et al., 2018c). Additionally, most of the co-existing species are known to be competitive ions, as they can compete with Cr ions ($HCrO_4^{2-}$) for surface sites on NMs. However, it has been observed that Na^+, K^+, Mg^{2+}, Ca^{2+}, Zn^{2+}, Cu^{2+}, Cd^{2+} do not significantly affect the sorptive removal of Cr (VI) (Bhaumik et al., 2016; Kera et al., 2017). The insignificant effects of co-existing cations are presumed to be due to the lower pH values of the working solution (e.g., pH 2–3).

In general, the higher sorptive removal of Cr ions could be due to the strong electrostatic attraction between negatively charged Cr ions (i.e., $HCrO_4^-$) and the positively charged surface of the NMs (Table 2).

Consequently, positively charged NMs may offer a repulsive force to the existing cations (e.g., Na^+, K^+, Mg^{2+}, Ca^{2+}, Zn^{2+}, Cu^{2+}, Cd^{2+}) to make most of their sorption sites available for Cr ions without competition (Ghernaout et al., 2011; Maitlo et al., 2019a). However, Cr ion removal efficiency may be distressed due to the co-existence of negatively charged species (e.g., F^-, Cl^-, NO_3^-, SO_4^{2-}, and CO_3^{2-}, and PO_4^{3-}). More specifically, these anions can be divided into diverse categories according to their competing effects on Cr removal efficiency. The presence of anions can lead to the formation of outer-sphere surface complexes with binding sites of the NMs. Such co-existing anions plausibly possess weaker adsorption affinity toward the sorptive sites of NMs than do Cr ions (Setshedi et al., 2015; Bhaumik et al., 2016; Maitlo et al., 2019c). Therefore, the presence of anions should not play a substantial role in the obstruction of the removal of aqueous Cr. On the other hand, the co-existence of high concentrations of CO_3^{2-} and PO_4^{3-} ions presents effective competition for the sorptive removal of Cr ions (Bhaumik et al., 2016; Maitlo et al., 2017; Maitlo et al., 2018a; Zhang et al., 2018c). The presence of these anions would produce inner-sphere surface complexes with binding surfaces of the NMs to occupy the available reactive sites of the NMs.

6.3. Performance comparison of adsorption and catalysis processes for Cr removal

Several conventional methods have been evaluated (refer to Section 3 for more details) as tools for the removal of aqueous Cr (Barrera-Díaz et al., 2012; Feng et al., 2018; Shaheen et al., 2018). Most of the established techniques suffer from technological and economic drawbacks, such as low pollutant-removal efficiency, lengthy operating times, high processing costs and electrical energy consumption, and the generation of large volumes of hazardous secondary pollutants (Kumar et al., 2017; Vellingiri et al., 2017; Maitlo et al., 2018b, 2019a). As a result, most of the better-known operating methods are uneconomical at large scales (Kobielska et al., 2018; Jin et al., 2019).

In this section, the real-world performance of the most preferred treatment approaches, including adsorption and photocatalysis (PEC)-based nanotechnology, was evaluated according to the most appropriate operating metrics, including maximum removal efficiency (%), electrical energy consumption ($kWh\,m^{-3}$), and maximum distribution coefficient ($mg\,g^{-1}\,\mu M^{-1}$) for aqueous Cr remediation (Table 3). Most of the PEC-based nanomaterials were uneconomical and ineffective at maintaining superior performance for the removal of aqueous Cr (Table 3). If the performance of PEC-based materials is assessed with respect to the maximum efficiency of Cr removal and electrical energy consumption, they can be ranked in the order: UV/TiO_2 (21.2–86%/232–663.71 $kWh{\cdot}m^{-3}$) > UV/Mg/TiO_2 (32.6%/152 $kWh{\cdot}m^{-3}$) > UV/ZnO (82.33%/478 $kWh{\cdot}m^{-3}$) > UV/Ag/TiO_2 (63.6%/71.42 $kWh{\cdot}m^{-3}$) > UV/Mg-Ag/TiO_2 (84.4%/30.31 $kWh{\cdot}m^{-3}$) (Table 3). In case of PEC techniques, PEC is an inefficient and energy-expensive process for complete removal of aqueous Cr (e.g., maximum Cr removal efficiency ranges from 21.2 to 86% and electrical energy consumption ranges from 30.31 to 663.71 $kWh\,m^{-3}$). Additionally, due to the poor removal efficiency of PEC systems, the final Cr concentration was considerably higher than the EPA-recommended level of 0.1 mg/L for chromium discharge into inland surface waters (Heffron et al., 2016; Shahid et al., 2017). Furthermore, such a chromium removal mechanism is complex and has been classified either by direct adsorption of aqueous Cr (VI) (in the case of NMs) or by photocatalytic reduction of Cr(VI) to Cr(III) (in the case of photocatalysis). In this regard, the relatively poor performance of PEC processes for the remediation of aqueous Cr(VI) ions is associated with the production of subsidiary byproducts (e.g., aqueous Cr(III) ions). As PEC techniques can only be used for the catalytic reduction of aqueous Cr(VI) to Cr(III) ions, PEC nanotechnology is not recommended as a remediation option for Cr.

In case of adsorption, most NMs exhibit enhanced adsorptive removal potential for aqueous Cr. The maximum Cr removal efficiency and maximum Kp values of NMs ranged from 93 to 99.99% and 106.2 to 1072.16 $mg\,g^{-1}\,\mu M^{-1}$, with no additional electrical energy consumption (Table 3). Adsorption-based nanotechnological approaches are therefore more practical and economically sustainable for the sorptive removal of contaminants such as Cr (e.g., Cr(VI) or Cr(III) ions) in water.

6.4. Challenges in nanotechnology for the sorptive removal of aqueous Cr

In general, the extensive applicability of advanced NMs has been investigated for the effective removal of Cr in aqueous systems. Conversely, to date, most of the advanced NMs have exhibited copious operating drawbacks such as (i) higher preparation cost, (ii) hydrolytic instability, (iii) oxidation and corrosion of transition metal oxide–based NMs under acidic conditions, (iv) the poor performance of certain (e.g., gold and silver) nanoparticles in the presence of interfering ions, (v) microscopically irreversible sorption, (vi) large amounts of toxic chemicals for NMs synthesis, (vii) low solubility/aggregation, (viii) the slow adsorption kinetics of organic polymeric material, and (ix) dissolution of natural polymers under acidic conditions. Among aforementioned issues, the cost-related ones (e.g., synthesis/regeneration cost) are yet the most important limiting factor for real-life applications (Maitlo et al., 2019b; Vikrant and Kim, 2019; Vikrant et al., 2019). Thus, most of aforementioned limiting issues or factors can be resolved through (i) the development of advanced, economic, or green synthesis approaches including agricultural/plant waste (e.g., bagasse pith, maize cob, coconut/peanut shell, and rice husk), mycelial microorganism (e.g., dictyophora indusiata and bacillus), and mineral slag (e.g., coal and fly ash) or through (ii) the optimization of the synthesis methodology, surface properties, better recyclability, and subsequent geometric arrangement of NMs (Vikrant and Kim, 2019; Wu et al., 2019). Consequently, for practical application of advanced NMs, interdisciplinary research efforts are desirable (e.g., active collaborations among environmental scientists, material engineers, and chemists) to overpower the recognized shortcomings.

7. Conclusion

In this review, we evaluated the potential for novel nanomaterials to remediate aqueous systems contaminated with Cr, with an emphasis on NM-based sorptive removal. We determined that advanced NMs should be more practical tools for the sorptive remediation of toxic heavy metals such as chromium due to their physical and chemical characteristics, including advantageous mechanical, electric, optical, and magnetic properties; extremely high aspect ratio; substantial surface area; small, hollow, layered structures; chemical stability; mesoporous framework; π-π electrostatic interactions; light mass density; functionalizing ligands; and strong binding energy.

Surface functionalities and the structural framework of the NMs are the major controls on sorptive removal potential of aqueous Cr. Most of these functionalities involve reactive anchoring sites for adsorption of Cr. However, to date, most advanced NMs (e.g., iron/iron oxide–based NMs, carbon-based nanostructures, covalent organic polymers, and MOFs) suffer from multiple limitations, including high preparation costs, hydrolytic instability, reactivation after adsorption saturation, microscopically irrevocable sorption, and selectivity challenges. Future research should examine new materials and recently introduced NMs (e.g., NMC-100, nZVI, Ppy-Go-NC, ppy/OMWCNTs, MM, Cu-BTC, and GSC) to determine whether they technically feasible cost-effective treatment options for the sorptive removal of toxic contaminants in aqueous systems.

Table 3
Comparison of Cr removal efficiencies and electrical energy consumption between sorption- and photocatalysis-based nanotechnology.

S. No	Adsorbent	Optimum adsorption condition (Temperature (°C, pH))	Initial Cr concentration (mg/L)	Sorbent dose (g/L)	Distribution coefficient ($mg\,g^{-1}\cdot\mu M$)	Maximum removal efficiency (%)	Final Cr concentration (mg/L)	Electric energy consumption (kWh/m^3)	Reference
[A] Photoelctrocatalysis									
1	UV/TiO_2	25, 7	5	1	–	58	2.1	664	(Shirzad Siboni et al., 2012)
2	UV/TiO_2	–	20	1	–	86.1	2.8	380	(Naimi-Joubani et al., 2015)
3	UV/TiO_2	35, 6	5	0.04	–	55.4	2.2	324	(Saien and Azizi, 2015)
4	UV/TiO_2	–	5	8	–	21.2	3.9	232	(Eskandarloo et al., 2014)
5	UV/ZnO	–	20	1	–	82.3	3.5	478	(Naimi-Joubani et al., 2015)
6	UV/Mg/TiO_2	–	5	8	–	32.6	3.4	152	(Eskandarloo et al., 2014)
7	UV/Ag/TiO_2	–	5	8	–	63.6	1.8	71.4	(Eskandarloo et al., 2014)
8	UV/Mg-Ag/TiO_2	–	5	8	–	84.4	0.8	30.3	(Eskandarloo et al., 2014)
[B] Adsorption									
1	nZVI	25, 3	60	0.5	1073	99.99	0.006	–	(Zhang et al., 2018c)
2	PPy/OMWCNTs	25, 2	350	0.5	437	99.99	0.035	–	(Bhaumik et al., 2016)
3	Ppy-GO-NC	25, 2	200	0.5	812	99.98	0.04	–	(Setshedi et al., 2015)
4	NMC-100	25, 1	1000	2.5	1041	99.99	0.1	–	(Cao et al., 2016)
5	GSC	40, 1.5	20	–	106	93	1.4	–	(Dubey et al., 2015)
6	F-MC	25, 1	1000	2.5	740	99.99	0.1	–	(Cao et al., 2017)
7	Cu-BTC	–, 7	20	–	125	99.9	0.02	–	(Maleki et al., 2015)

Acknowledgements

The authors acknowledge support made by the National Research Foundation of Korea funded by the Ministry of Science, ICT and Future Planning (Grant No: 2016R1E1A1A01940995).

References

Aboutorabi, L., Morsali, A., Tahmasebi, E., Buyukgungor, O., 2016. Metal–organic framework based on isonicotinate N-oxide for fast and highly efficient aqueous phase Cr (VI) adsorption. Inorg. Chem. 55, 5507–5513.

Ali, I., Kim, J.-O., 2018. Visible-light-assisted photocatalytic activity of bismuth-TiO_2 nanotube composites for chromium reduction and dye degradation. Chemosphere 207, 285–292.

Angelucci, D.M., Stazi, V., Daugulis, A.J., Tomei, M.C., 2017. Treatment of synthetic tannery wastewater in a continuous two-phase partitioning bioreactor: biodegradation of the organic fraction and chromium separation. J. Clean. Prod. 152, 321–329.

Anupam, K., Dutta, S., Bhattacharjee, C., Datta, S., 2011. Adsorptive removal of chromium (VI) from aqueous solution over powdered activated carbon: optimisation through response surface methodology. Chem. Eng. J. 173, 135–143.

Aoudj, S., Cheknane, B., Zemmouri, H., Zermane, F., Khelifa, A., Hecini, M., Drouiche, N., 2017. Kinetics and adsorption isotherm for the removal of fluoride and chromium (VI) from wastewater by electrocoagulation. Desalin. Water Treat. 82, 262–270.

Arain, M.B., Ali, I., Yilmaz, E., Soylak, M., 2018. Nanomaterial's based chromium speciation in environmental samples: a review. TrAC Trends Anal. Chem. 103, 44–55.

Aroua, M.K., Zuki, F.M., Sulaiman, N.M., 2007. Removal of chromium ions from aqueous solutions by polymer-enhanced ultrafiltration. J. Hazard. Mater. 147, 752–758.

Asri, M., El Ghachtouli, N., Elabed, S., Koraichi, S.I., Elabed, A., Silva, B., Tavares, T., 2018. Wicherhamomyces anomalus biofilm supported on wood husk for chromium wastewater treatment. J. Hazard. Mater. 359, 554–562.

Athanasekou, C., Romanos, G.E., Papageorgiou, S., Manolis, G., Katsaros, F., Falaras, P., 2017. Photocatalytic degradation of hexavalent chromium emerging contaminant via advanced titanium dioxide nanostructures. Chem. Eng. J. 318, 171–180.

Attia, A., Khedr, S., Elkholy, S., 2010. Adsorption of chromium ion (VI) by acid activated carbon. Braz. J. Chem. Eng. 27, 183–193.

Aulakh, M.S., Khurana, M.P.S., Singh, D., 2009. Water pollution related to agricultural, industrial, and urban activities, and its effects on the food chain: case studies from Punjab. J. New Seeds 10, 112–137.

Barrera-Díaz, C.E., Lugo-Lugo, V., Bilyeu, B., 2012. A review of chemical, electrochemical and biological methods for aqueous Cr (VI) reduction. J. Hazard. Mater. 223, 1–12.

Bentchikou, L., Mechelouf, F.-Z., Neggaz, F., Mellah, A., 2017. Removal of hexavalent chromium from water by using natural brown clay. Journal of the Turkish Chemical Society, Section B: Chemical Engineering 1, 43–52.

Bhaumik, M., Agarwal, S., Gupta, V.K., Maity, A., 2016. Enhanced removal of Cr (VI) from aqueous solutions using polypyrrole wrapped oxidized MWCNTs nanocomposites adsorbent. J. Colloid Interface Sci. 470, 257–267.

Burakov, A.E., Galunin, E.V., Burakova, I.V., Kucherova, A.E., Agarwal, S., Tkachev, A.G., Gupta, V.K., 2018. Adsorption of heavy metals on conventional and nanostructured materials for wastewater treatment purposes: a review. Ecotoxicol. Environ. Saf. 148, 702–712.

Cai, F., Liu, X., Liu, S., Liu, H., Huang, Y., 2014. A simple one-pot synthesis of highly fluorescent nitrogen-doped graphene quantum dots for the detection of Cr(vi) in aqueous media. RSC Adv. 4, 52016–52022.

Cao, Y., Huang, J., Li, Y., Qiu, S., Liu, J., Khasanov, A., Khan, M.A., Young, D.P., Peng, F., Cao, D., 2016. One-pot melamine derived nitrogen doped magnetic carbon nanoadsorbents with enhanced chromium removal. Carbon 109, 640–649.

Cao, Y., Huang, J., Peng, X., Cao, D., Galaska, A., Qiu, S., Liu, J., Khan, M.A., Young, D.P., Ryu, J.E., Feng, H., Yerra, N., Guo, Z., 2017. Poly(vinylidene fluoride) derived fluorine-doped magnetic carbon nanoadsorbents for enhanced chromium removal. Carbon 115, 503–514.

Chansuvarn, W., Jainae, K., 2018. Determination of contaminated heavy metals in lacquer thinner. In: Applied Mechanics and Materials. Trans Tech Publ, pp. 144–148.

Chen, G., Feng, J., Wang, W., Yin, Y., Liu, H., 2017. Photocatalytic removal of hexavalent chromium by newly designed and highly reductive TiO_2 nanocrystals. Water Res. 108, 383–390.

Chen, Z., Wei, D., Li, Q., Wang, X., Yu, S., Liu, L., Liu, B., Xie, S., Wang, J., Chen, D., Hayat, T., Wang, X., 2018. Macroscopic and microscopic investigation of Cr(VI) immobilization by nanoscaled zero-valent iron supported zeolite MCM-41 via batch, visual, XPS and EXAFS techniques. J. Clean. Prod. 181, 745–752.

Chrysochoou, M., Johnston, C.P., 2012. Reduction of chromium (VI) in saturated zone sediments by calcium polysulfide and nanoscale zerovalent iron derived from green tea extract. In: GeoCongress 2012: State of the Art and Practice in Geotechnical Engineering, pp. 3959–3967.

Cieslak Golonka, M., 1996. Toxic and mutagenic effects of chromium (VI). A review. Polyhedron 15, 3667–3689.

Coetzee, J.J., Bansal, N., Chirwa, E.M., 2018. Chromium in environment, its toxic effect from chromite-mining and ferrochrome industries, and its possible bioremediation. Exposure and Health 1–12.

D'Angelo, A., Galia, A., Scialdone, O., 2015. Cathodic abatement of Cr (VI) in water by microbial reverse-electrodialysis cells. J. Electroanal. Chem. 748, 40–46.

Dehghani, M.H., Taher, M.M., Bajpai, A.K., Heibati, B., Tyagi, I., Asif, M., Agarwal, S., Gupta, V.K., 2015. Removal of noxious Cr (VI) ions using single-walled carbon nanotubes and multi-walled carbon nanotubes. Chem. Eng. J. 279, 344–352.

Dhal, B., Thatoi, H., Das, N., Pandey, B., 2013. Chemical and microbial remediation of hexavalent chromium from contaminated soil and mining/metallurgical solid waste: a review. J. Hazard. Mater. 250, 272–291.

Dubey, R., Bajpai, J., Bajpai, A., 2015. Green synthesis of graphene sand composite (GSC) as novel adsorbent for efficient removal of Cr (VI) ions from aqueous solution. Journal of water process engineering 5, 83–94.

Eskandarloo, H., Badiei, A., Behnajady, M.A., Ziarani, G.M., 2014. Minimization of electrical energy consumption in the photocatalytic reduction of Cr(vi) by using immobilized Mg, Ag co-impregnated TiO_2 nanoparticles. RSC Adv. 4, 28587–28596.

Espallargas, G.M., Coronado, E., 2018. Magnetic functionalities in MOFs: from the framework to the pore. Chem. Soc. Rev. 47, 533–557.

Fang, W., Jiang, X., Luo, H., Geng, J., 2018a. Synthesis of graphene/SiO_2@polypyrrole nanocomposites and their application for Cr(VI) removal in aqueous solution. Chemosphere 197, 594–602.

Fang, Y., Wen, J., Zeng, G., Jia, F., Zhang, S., Peng, Z., Zhang, H., 2018b. Effect of mineralizing agents on the adsorption performance of metal–organic framework MIL-100(Fe) towards chromium(VI). Chem. Eng. J. 337, 532–540.

Fellenz, N., Perez-Alonso, F.J., Martin, P.P., García-Fierro, J.L., Bengoa, J.F., Marchetti, S.G., Rojas, S., 2017. Chromium (VI) removal from water by means of adsorption-reduction at the surface of amino-functionalized MCM-41 sorbents. Microporous Mesoporous Mater. 239, 138–146.

Feng, M., Zhang, P., Zhou, H.-C., Sharma, V.K., 2018. Water-stable metal-organic frameworks for aqueous removal of heavy metals and radionuclides: a review. Chemosphere 209, 783–800.

Foo, K.Y., Hameed, B.H., 2010. Insights into the modeling of adsorption isotherm systems. Chem. Eng. J. 156, 2–10.

Ghernaout, D., Naceur, M., Ghernaout, B., 2011. A review of electrocoagulation as a promising coagulation process for improved organic and inorganic matters removal by electrophoresis and electroflotation. Desalin. Water Treat. 28, 287–320.

Ghosh, A., Dastidar, M.G., Sreekrishnan, T., 2018. Bioremediation of Chromium Complex Dye by Growing Aspergillus flavus. Water Quality Management. Springer, pp. 81–92.

Gong, K., Hu, Q., Yao, L., Li, M., Sun, D., Shao, Q., Qiu, B., Guo, Z., 2018. Ultrasonic pretreated sludge derived stable magnetic active carbon for Cr(VI) removal from wastewater. ACS Sustain. Chem. Eng. 6, 7283–7291.

Guan, Q., Wu, D., Lin, Y., Chen, X., Wang, X., Li, C., He, S., Kong, H., 2009. Application of zeolitic material synthesized from thermally treated sediment to the removal of trivalent chromium from wastewater. J. Hazard. Mater. 167, 244–249.

Gupta, V.K., Gupta, M., Sharma, S., 2001. Process development for the removal of lead and chromium from aqueous solutions using red mud - an aluminium industry waste. Water Res. 35, 1125–1134.

Gupta, V.K., Agarwal, S., Saleh, T.A., 2011. Chromium removal by combining the magnetic properties of iron oxide with adsorption properties of carbon nanotubes. Water Res. 45, 2207–2212.

Haktanır, C., Özbelge, H.Ö., Bıçak, N., Yılmaz, L., 2017. Removal of hexavalent chromium anions via polymer enhanced ultrafiltration using a fully ionized polyelectrolyte. Sep. Sci. Technol. 52, 2487–2497.

He, C., Yang, Z., Ding, J., Chen, Y., Tong, X., Li, Y., 2017. Effective removal of Cr(VI) from aqueous solution by 3-aminopropyltriethoxysilane-functionalized graphene oxide. Colloids Surf. A Physicochem. Eng. Asp. 520, 448–458.

Heffron, J., Marhefke, M., Mayer, B.K., 2016. Removal of trace metal contaminants from potable water by electrocoagulation. Sci. Rep. 6, 28478.

Herrero-Latorre, C., Barciela-García, J., García-Martín, S., Pena-Crecente, R., 2017. Graphene and carbon nanotubes as solid phase extraction sorbents for the speciation of chromium: a review. Anal. Chim. Acta 1002, 1–17.

Heydari, S., Sharififard, H., Nabavinia, M., Kiani, H., Parvizi, M., 2013. Adsorption of chromium ions from aqueous solution by carbon adsorbent. International Journal of Environmental, Chemical, Ecological, Geological And Geophysical Engineering 7, 649–652.

Huang, Z.-n., Wang, X.-l., Yang, D.-s., 2015. Adsorption of Cr(VI) in wastewater using magnetic multi-wall carbon nanotubes. Water Science and Engineering 8, 226–232.

Huang, J., Cao, Y., Shao, Q., Peng, X., Guo, Z., 2017. Magnetic nanocarbon adsorbents with enhanced hexavalent chromium removal: morphology dependence of fibrillar vs particulate structures. Ind. Eng. Chem. Res. 56, 10689–10701.

Huang, J., Li, Y., Cao, Y., Peng, F., Cao, Y., Shao, Q., Liu, H., Guo, Z., 2018. Hexavalent chromium removal over magnetic carbon nanoadsorbents: synergistic effect of fluorine and nitrogen co-doping. J. Mater. Chem. A 6, 13062–13074.

Jain, M., Yadav, M., Kohout, T., Lahtinen, M., Garg, V.K., Sillanpää, M., 2018. Development of iron oxide/activated carbon nanoparticle composite for the removal of Cr(VI), Cu(II) and Cd(II) ions from aqueous solution. Water Resources and Industry 20, 54–74.

Janik, P., Zawisza, B., Talik, E., Sitko, R., 2018. Selective adsorption and determination of hexavalent chromium ions using graphene oxide modified with amino silanes. Microchim. Acta 185, 117.

Jiang, W., Pelaez, M., Dionysiou, D.D., Entezari, M.H., Tsoutsou, D., O'Shea, K., 2013. Chromium(VI) removal by maghemite nanoparticles. Chem. Eng. J. 222, 527–533.

Jiang, Y., Liu, Z., Zeng, G., Liu, Y., Shao, B., Li, Z., Liu, Y., Zhang, W., He, Q., 2018. Polyaniline-based adsorbents for removal of hexavalent chromium from aqueous solution: a mini review. Environ. Sci. Pollut. Res. 25, 6158–6174.

Jin, W., Du, H., Zheng, S., Zhang, Y., 2016. Electrochemical processes for the environmental remediation of toxic Cr (VI): a review. Electrochim. Acta 191, 1044–1055.

Jin, L., Huang, L., Ren, L., He, Y., Tang, J., Wang, S., Yang, W., Wang, H., Chai, L., 2019. Preparation of stable and high-efficient poly(m-phenylenediamine)/reduced graphene oxide composites for hexavalent chromium removal. J. Mater. Sci. 54, 383–395.

Kang, H., Cheng, Z., Lai, H., Ma, H., Liu, Y., Mai, X., Wang, Y., Shao, Q., Xiang, L., Guo, X., Guo, Z., 2018. Superlyophobic anti-corrosive and self-cleaning titania robust mesh

membrane with enhanced oil/water separation. Sep. Purif. Technol. 201, 193–204.
Karthikeyan, T., Rajgopal, S., Miranda, L.R., 2005. Chromium (VI) adsorption from aqueous solution by Hevea Brasilinesis sawdust activated carbon. J. Hazard. Mater. 124, 192–199.
Kera, N.H., Bhaumik, M., Pillay, K., Ray, S.S., Maity, A., 2017. Selective removal of toxic Cr(VI) from aqueous solution by adsorption combined with reduction at a magnetic nanocomposite surface. J. Colloid Interface Sci. 503, 214–228.
Keshmirizadeh, E., Yousefi, S., Rofouei, M.K., 2011. An investigation on the new operational parameter effective in Cr(VI) removal efficiency: a study on electrocoagulation by alternating pulse current. J. Hazard. Mater. 190, 119–124.
Khan, A., Szulejko, J.E., Kim, K.-H., Sammadar, P., Lee, S.S., Yang, X., Ok, Y.S., 2019. A comparison of figure of merit (FOM) for various materials in adsorptive removal of benzene under ambient temperature and pressure. Environ. Res. 168, 96–108.
Kim, M.K., Shanmuga Sundaram, K., Anantha Iyengar, G., Lee, K.-P., 2015. A novel chitosan functional gel included with multiwall carbon nanotube and substituted polyaniline as adsorbent for efficient removal of chromium ion. Chem. Eng. J. 267, 51–64.
Kobielska, P.A., Howarth, A.J., Farha, O.K., Nayak, S., 2018. Metal–organic frameworks for heavy metal removal from water. Coord. Chem. Rev. 358, 92–107.
Kraus, M., Trommler, U., Holzer, F., Kopinke, F.-D., Roland, U., 2018. Competing adsorption of toluene and water on various zeolites. Chem. Eng. J. 351, 356–363.
Kukkar, D., Vellingiri, K., Kumar, V., Deep, A., Kim, K.-H., 2018. A critical review on the metal sensing capabilities of optically active nanomaterials: limiting factors, mechanism, and performance evaluation. TrAC Trends Anal. Chem. 109, 227–246.
Kumar, P.A., Ray, M., Chakraborty, S., 2007. Hexavalent chromium removal from wastewater using aniline formaldehyde condensate coated silica gel. J. Hazard. Mater. 143, 24–32.
Kumar, P., Vellingiri, K., Kim, K.-H., Brown, R.J.C., Manos, M.J., 2017. Modern progress in metal-organic frameworks and their composites for diverse applications. Microporous Mesoporous Mater. 253, 251–265.
Kuppusamy, S., Jayaraman, N., Jagannathan, M., Kadarkarai, M., Aruliah, R., 2017. Electrochemical decolorization and biodegradation of tannery effluent for reduction of chemical oxygen demand and hexavalent chromium. Journal of Water Process Engineering 20, 22–28.
Labied, R., Benturki, O., Eddine Hamitouche, A.Y., Donnot, A., 2018. Adsorption of hexavalent chromium by activated carbon obtained from a waste lignocellulosic material (Ziziphus jujuba cores): kinetic, equilibrium, and thermodynamic study. Adsorption Science & Technology 36, 1066–1099.
Lai, K.C.K., Lo, I.M.C., 2008. Removal of chromium (VI) by acid-washed zero-valent iron under various groundwater geochemistry conditions. Environmental Science & Technology 42, 1238–1244.
Laxman, R.S., More, S., 2002. Reduction of hexavalent chromium by Streptomyces griseus. Miner. Eng. 15, 831–837.
Lee, C.-G., Lee, S., Park, J.-A., Park, C., Lee, S.J., Kim, S.-B., An, B., Yun, S.-T., Lee, S.-H., Choi, J.-W., 2017. Removal of copper, nickel and chromium mixtures from metal plating wastewater by adsorption with modified carbon foam. Chemosphere 166, 203–211.
Le-Minh, N., Sivret, E.C., Shammay, A., Stuetz, R.M., 2018. Factors affecting the adsorption of gaseous environmental odors by activated carbon: a critical review. Crit. Rev. Environ. Sci. Technol. 48, 341–375.
Leo, A., Hansch, C., Elkins, D., 1971. Partition coefficients and their uses. Chem. Rev. 71, 525–616.
Li, Y., Zhu, S., Liu, Q., Chen, Z., Gu, J., Zhu, C., Lu, T., Zhang, D., Ma, J., 2013. N-doped porous carbon with magnetic particles formed in situ for enhanced Cr(VI) removal. Water Res. 47, 4188–4197.
Li, X., Gao, X., Ai, L., Jiang, J., 2015. Mechanistic insight into the interaction and adsorption of Cr(VI) with zeolitic imidazolate framework-67 microcrystals from aqueous solution. Chem. Eng. J. 274, 238–246.
Li, L.-L., Feng, X.-Q., Han, R.-P., Zang, S.-Q., Yang, G., 2017. Cr (VI) removal via anion exchange on a silver-triazolate MOF. J. Hazard. Mater. 321, 622–628.
Li, M., Zhou, S., Xu, Y., Liu, Z., Ma, F., Zhi, L., Zhou, X., 2018a. Simultaneous Cr (VI) reduction and bioelectricity generation in a dual chamber microbial fuel cell. Chem. Eng. J. 334, 1621–1629.
Li, Z., Wang, B., Qin, X., Wang, Y., Liu, C., Shao, Q., Wang, N., Zhang, J., Wang, Z., Shen, C., Guo, Z., 2018b. Superhydrophobic/superoleophilic polycarbonate/carbon nanotubes porous monolith for selective oil adsorption from water. ACS Sustain. Chem. Eng. 6, 13747–13755.
Liang, Q., Luo, H., Geng, J., Chen, J., 2018. Facile one-pot preparation of nitrogen-doped ultra-light graphene oxide aerogel and its prominent adsorption performance of Cr (VI). Chem. Eng. J. 338, 62–71.
Lin, F., Wang, Y., Lin, Z., 2016. One-pot synthesis of nitrogen-enriched carbon spheres for hexavalent chromium removal from aqueous solution. RSC Adv. 6, 33055–33062.
Liou, Y.H., Lo, S.-L., Lin, C.-J., Kuan, W.H., Weng, S.C., 2005. Effects of iron surface pretreatment on kinetics of aqueous nitrate reduction. J. Hazard. Mater. 126, 189–194.
Lu, J., Xu, K., Yang, J., Hao, Y., Cheng, F., 2017a. Nano iron oxide impregnated in chitosan bead as a highly efficient sorbent for Cr(VI) removal from water. Carbohydr. Polym. 173, 28–36.
Lu, W., Li, J., Sheng, Y., Zhang, X., You, J., Chen, L., 2017b. One-pot synthesis of magnetic iron oxide nanoparticle-multiwalled carbon nanotube composites for enhanced removal of Cr(VI) from aqueous solution. J. Colloid Interface Sci. 505, 1134–1146.
Lukina, A., Boutin, C., Rowland, O., Carpenter, D., 2016. Evaluating trivalent chromium toxicity on wild terrestrial and wetland plants. Chemosphere 162, 355–364.
Luo, C., Tian, Z., Yang, B., Zhang, L., Yan, S., 2013. Manganese dioxide/iron oxide/acid oxidized multi-walled carbon nanotube magnetic nanocomposite for enhanced hexavalent chromium removal. Chem. Eng. J. 234, 256–265.
Lupa, L., Maranescu, B., Visa, A., 2018. Equilibrium and kinetic studies of chromium ions adsorption on Co (II)-based phosphonate metal organic frameworks. Sep. Sci. Technol. 53, 1017–1026.
Machado, S., Stawiński, W., Slonina, P., Pinto, A.R., Grosso, J.P., Nouws, H.P.A., Albergaria, J.T., Delerue-Matos, C., 2013. Application of green zero-valent iron nanoparticles to the remediation of soils contaminated with ibuprofen. Sci. Total Environ. 461-462, 323–329.
Maitlo, H.A., Kim, J.H., Park, J.Y., 2017. Arsenic treatment and power generation with a dual-chambered fuel cell with anionic and cationic membranes using NaHCO3 anolyte and HCl or NaCl catholyte. Chemosphere 172, 138–146.
Maitlo, H.A., Kim, J.H., An, B.M., Park, J.Y., 2018a. Effects of supporting electrolytes in treatment of arsenate-containing wastewater with power generation by aluminumair fuel cell electrocoagulation. J. Ind. Eng. Chem. 57, 254–262.
Maitlo, H.A., Kim, J.H., Kim, K.-H., Park, J.Y., Khan, A., 2018b. Metal-air fuel cell electrocoagulation techniques for the treatment of arsenic in water. J. Clean. Prod. 207, 67–84.
Maitlo, H.A., Kim, J.H., Kim, K.-H., Park, J.Y., Khan, A., 2019a. Metal-air fuel cell electrocoagulation techniques for the treatment of arsenic in water. J. Clean. Prod. 207, 67–84.
Maitlo, H.A., Kim, K.-H., Khan, A., Szulejko, J.E., Kim, J.C., Song, H.N., Ahn, W.-S., 2019b. Competitive adsorption of gaseous aromatic hydrocarbons in a binary mixture on nanoporous covalent organic polymers at various partial pressures. Environ. Res. 173, 1–11.
Maitlo, H.A., Kim, K.-H., Yang Park, J., Hwan Kim, J., 2019c. Removal mechanism for chromium (VI) in groundwater with cost-effective iron-air fuel cell electrocoagulation. Sep. Purif. Technol. 213, 378–388.
Maitlo, H.A., Lee, J., Park, J.Y., Kim, J.-C., Kim, K.-H., Kim, J.H., 2019d. An energy-efficient air-breathing cathode electrocoagulation approach for the treatment of arsenite in aquatic systems. J. Ind. Eng. Chem. 73, 205–213.
Malaviya, P., Singh, A., 2016. Bioremediation of chromium solutions and chromium containing wastewaters. Crit. Rev. Microbiol. 42, 607–633.
Maleki, A., Hayati, B., Naghizadeh, M., Joo, S.W., 2015. Adsorption of hexavalent chromium by metal organic frameworks from aqueous solution. J. Ind. Eng. Chem. 28, 211–216.
Martin, P.P., Agosto, M.F., Bengoa, J.F., Fellenz, N.A., 2017. Zinc and Chromium elimination from complex aqueous matrices using a unique aminopropyl-modified MCM-41 sorbent: temperature, kinetics and selectivity studies. Journal of Environmental Chemical Engineering 5, 1210–1218.
Mishra, S., Chowdhary, P., Bharagava, R.N., 2019. Conventional methods for the removal of industrial pollutants, their merits and demerits. In: Emerging and Eco-friendly Approaches for Waste Management. Springer, pp. 1–31.
Mohan, D., Pittman Jr., C.U., 2006. Activated carbons and low cost adsorbents for remediation of tri- and hexavalent chromium from water. J. Hazard. Mater. 137, 762–811.
Mullick, A., Moulik, S., Bhattacharjee, S., 2018. Removal of hexavalent chromium from aqueous solutions by low-cost rice husk-based activated carbon: kinetic and thermodynamic studies. Indian Chemical Engineer 60, 58–71.
Muthumareeswaran, M., Alhoshan, M., Agarwal, G.P., 2017. Ultrafiltration membrane for effective removal of chromium ions from potable water. Sci. Rep. 7, 41423.
Naimi-Joubani, M., Shirzad-Siboni, M., Yang, J.-K., Gholami, M., Farzadkia, M., 2015. Photocatalytic reduction of hexavalent chromium with illuminated ZnO/TiO_2 composite. J. Ind. Eng. Chem. 22, 317–323.
Nasrollahpour, A., Moradi, S.E., 2017. Hexavalent chromium removal from water by ionic liquid modified metal-organic frameworks adsorbent. Microporous Mesoporous Mater. 243, 47–55.
Nigar, H., Julián, I., Mallada, R., Santamaría, J., 2018. Microwave-assisted catalytic combustion for the efficient continuous cleaning of VOC-containing air streams. Environmental Science & Technology 52, 5892–5901.
Pan, D., Ge, S., Zhang, X., Mai, X., Li, S., Guo, Z., 2018a. Synthesis and photoelectrocatalytic activity of In_2O_3 hollow microspheres via a bio-template route using yeast templates. Dalton Trans. 47, 708–715.
Pan, D., Ge, S., Zhao, J., Shao, Q., Guo, L., Zhang, X., Lin, J., Xu, G., Guo, Z., 2018b. Synthesis, characterization and photocatalytic activity of mixed-metal oxides derived from NiCoFe ternary layered double hydroxides. Dalton Trans. 47, 9765–9778.
Pan, D., Ge, S., Zhao, J., Tian, J., Shao, Q., Guo, L., Mai, X., Wu, T., Murugadoss, V., Liu, H., Ding, T., Angaiah, S., Guo, Z., 2019. Synthesis and characterization of ZnNiIn layered double hydroxides derived mixed metal oxides with highly efficient photoelectrocatalytic activities. Ind. Eng. Chem. Res. 58, 836–848.
Peng, W., Li, H., Liu, Y., Song, S., 2017. A review on heavy metal ions adsorption from water by graphene oxide and its composites. J. Mol. Liq. 230, 496–504.
Peters, R.W., Walker, T.J., Eriksen, E., 1985. Wastewater treatment - physical and chemical methods. J. Water Pollut. Control Fed. 57, 503–517.
Pillay, K., Cukrowska, E.M., Coville, N.J., 2009. Multi-walled carbon nanotubes as adsorbents for the removal of parts per billion levels of hexavalent chromium from aqueous solution. J. Hazard. Mater. 166, 1067–1075.
Poornima, K., Karthik, L., Swadhini, S., Mythili, S., Sathiavelu, A., 2010. Degradation of chromium by using a novel strains of Pseudomonas species. Journal of Microbial and Biochemical Technology 2.
Pradhan, D., Sukla, L.B., Sawyer, M., Rahman, P.K., 2017. Recent bioreduction of hexavalent chromium in wastewater treatment: a review. J. Ind. Eng. Chem. 55, 1–20.
Puthiaraj, P., Lee, Y.-R., Ahn, W.-S., 2017. Microporous amine-functionalized aromatic polymers and their carbonized products for CO_2 adsorption. Chem. Eng. J. 319, 65–74.
Qurie, M., Khamis, M., Manassra, A., Ayyad, I., Nir, S., Scrano, L., Bufo, S.A., Karaman, R., 2013. Removal of Cr (VI) from aqueous environments using micelle-clay adsorption. Sci. World J. 2013.

Raji, C., Anirudhan, T., 1998. Batch Cr (VI) removal by polyacrylamide-grafted sawdust: kinetics and thermodynamics. Water Res. 32, 3772–3780.
Ramesha, G.K., Vijaya Kumara, A., Muralidhara, H.B., Sampath, S., 2011. Graphene and graphene oxide as effective adsorbents toward anionic and cationic dyes. J. Colloid Interface Sci. 361, 270–277.
Rao, A., Bankar, A., Kumar, A.R., Gosavi, S., Zinjarde, S., 2013. Removal of hexavalent chromium ions by Yarrowia lipolytica cells modified with phyto-inspired Fe0/Fe3O4 nanoparticles. J. Contam. Hydrol. 146, 63–73.
Reddy, K.R., Cameselle, C., 2009. Electrochemical Remediation Technologies for Polluted Soils, Sediments and Groundwater. John Wiley & Sons.
Ren, G., Wang, X., Huang, P., Zhong, B., Zhang, Z., Yang, L., Yang, X., 2017. Chromium (VI) adsorption from wastewater using porous magnetite nanoparticles prepared from titanium residue by a novel solid-phase reduction method. Sci. Total Environ. 607-608, 900–910.
Ren, L., Dong, J., Chi, Z., Huang, H., 2018. Reduced graphene oxide-nano zero value iron (rGO-nZVI) micro-electrolysis accelerating Cr(VI) removal in aquifer. J. Environ. Sci. 73, 96–106.
Rengaraj, S., Yeon, K.-H., Moon, S.-H., 2001. Removal of chromium from water and wastewater by ion exchange resins. J. Hazard. Mater. 87, 273–287.
Rodríguez, R., Espada, J., Gallardo, M., Molina, R., López-Muñoz, M., 2018. Life cycle assessment and techno-economic evaluation of alternatives for the treatment of wastewater in a chrome-plating industry. J. Clean. Prod. 172, 2351–2362.
Saien, J., Azizi, A., 2015. Simultaneous photocatalytic treatment of Cr (VI), Ni (II) and SDBS in aqueous solutions: evaluation of removal efficiency and energy consumption. Process Saf. Environ. Prot. 95, 114–125.
Salam, M.A., 2017. Preparation and characterization of chitin/magnetite/multiwalled carbon nanotubes magnetic nanocomposite for toxic hexavalent chromium removal from solution. J. Mol. Liq. 233, 197–202.
Samuel, M.S., Subramaniyan, V., Bhattacharya, J., Chidambaram, R., Qureshi, T., Pradeep Singh, N.D., 2018a. Ultrasonic-assisted synthesis of graphene oxide – fungal hyphae: an efficient and reclaimable adsorbent for chromium(VI) removal from aqueous solution. Ultrason. Sonochem. 48, 412–417.
Samuel, M.S., Subramaniyan, V., Bhattacharya, J., Parthiban, C., Chand, S., Singh, N.D.P., 2018b. A GO-CS@MOF [Zn(BDC)(DMF)] material for the adsorption of chromium (VI) ions from aqueous solution. Compos. Part B 152, 116–125.
Samuel, M.S., Bhattacharya, J., Raj, S., Santhanam, N., Singh, H., Pradeep Singh, N.D., 2019. Efficient removal of Chromium(VI) from aqueous solution using chitosan grafted graphene oxide (CS-GO) nanocomposite. Int. J. Biol. Macromol. 121, 285–292.
Sane, P., Chaudhari, S., Nemade, P., Sontakke, S., 2018. Photocatalytic reduction of chromium (VI) using combustion synthesized TiO2. Journal of Environmental Chemical Engineering 6, 68–73.
Sarkar, B., Mandal, S., Tsang, Y.F., Kumar, P., Kim, K.-H., Ok, Y.S., 2018. Designer carbon nanotubes for contaminant removal in water and wastewater: a critical review. Sci. Total Environ. 612, 561–581.
Schweitzer, L., Noblet, J., 2018. Water contamination and pollution. In: Green Chemistry. Elsevier, pp. 261–290.
Scialdone, O., D'Angelo, A., De Lumè, E., Galia, A., 2014. Cathodic reduction of hexavalent chromium coupled with electricity generation achieved by reverse-electrodialysis processes using salinity gradients. Electrochim. Acta 137, 258–265.
Setshedi, K.Z., Bhaumik, M., Onyango, M.S., Maity, A., 2015. High-performance towards Cr (VI) removal using multi-active sites of polypyrrole–graphene oxide nanocomposites: batch and column studies. Chem. Eng. J. 262, 921–931.
Shaban, M., Abukhadra, M.R., Rabia, M., Elkader, Y.A., Abd El-Halim, M.R., 2018. Investigation the adsorption properties of graphene oxide and polyaniline nano/micro structures for efficient removal of toxic Cr(VI) contaminants from aqueous solutions; kinetic and equilibrium studies. Rendiconti Lincei. Scienze Fisiche e Naturali 29, 141–154.
Shaheen, S.M., Niazi, N.K., Hassan, N.E., Bibi, I., Wang, H., Tsang, D.C., Ok, Y.S., Bolan, N., Rinklebe, J., 2018. Wood-based biochar for the removal of potentially toxic elements in water and wastewater: a critical review. Int. Mater. Rev. 1–32.
Shahid, M., Shamshad, S., Rafiq, M., Khalid, S., Bibi, I., Niazi, N.K., Dumat, C., Rashid, M.I., 2017. Chromium speciation, bioavailability, uptake, toxicity and detoxification in soil-plant system: a review. Chemosphere 178, 513–533.
Shakya, M., Rene, E.R., Nancharaiah, Y.V., Lens, P.N.L., 2018. Fungal-based nanotechnology for heavy metal removal. In: Gothandam, K.M., Ranjan, S., Dasgupta, N., Ramalingam, C., Lichtfouse, E. (Eds.), Nanotechnology, Food Security and Water Treatment. Springer International Publishing, Cham, pp. 229–253.
Sheikhmohammadi, A., Mohseni, S.M., Khodadadi, R., Sardar, M., Abtahi, M., Mahdavi, S., Keramati, H., Dahaghin, Z., Rezaei, S., Almasian, M., Sarkhosh, M., Faraji, M., Nazari, S., 2017. Application of graphene oxide modified with 8-hydroxyquinoline for the adsorption of Cr (VI) from wastewater: optimization, kinetic, thermodynamic and equilibrium studies. J. Mol. Liq. 233, 75–88.
Shirzad Siboni, M., Samadi, M.-T., Yang, J.-K., Lee, S.-M., 2012. Photocatalytic removal of Cr (VI) and Ni (II) by UV/TiO_2: kinetic study. Desalin. Water Treat. 40, 77–83.
Solís-Fernández, P., Rozada, R., Paredes, J.I., Villar-Rodil, S., Fernández-Merino, M.J., Guardia, L., Martínez-Alonso, A., Tascón, J.M.D., 2012. Chemical and microscopic analysis of graphene prepared by different reduction degrees of graphene oxide. J. Alloys Compd. 536, S532–S537.
Song, B., Wang, T., Sun, H., Shao, Q., Zhao, J., Song, K., Hao, L., Wang, L., Guo, Z., 2017. Two-step hydrothermally synthesized carbon nanodots/WO3 photocatalysts with enhanced photocatalytic performance. Dalton Trans. 46, 15769–15777.
Sun, J.M., Li, F., Huang, J.C., 2006. Optimum pH for Cr^{6+} Co-removal with mixed Cu^{2+}, Zn^{2+}, and Ni^{2+} precipitation. Ind. Eng. Chem. Res. 45, 1557–1562.
Sun, S., Zhu, L., Liu, X., Wu, L., Dai, K., Liu, C., Shen, C., Guo, X., Zheng, G., Guo, Z., 2018. Superhydrophobic shish-kebab membrane with self-cleaning and oil/water separation properties. ACS Sustain. Chem. Eng. 6, 9866–9875.
Szulejko, J.E., Kim, K.-H., Parise, J., 2018. Seeking the most powerful and practical real-world sorbents for gaseous benzene as a representative volatile organic compound based on performance metrics. Sep. Purif. Technol. 212, 980–985.
Tian, J., Shao, Q., Zhao, J., Pan, D., Dong, M., Jia, C., Ding, T., Wu, T., Guo, Z., 2019. Microwave solvothermal carboxymethyl chitosan templated synthesis of TiO_2/ZrO_2 composites toward enhanced photocatalytic degradation of Rhodamine B. J. Colloid Interface Sci. 541, 18–29.
Tran, H.N., You, S.-J., Chao, H.-P., 2016. Thermodynamic parameters of cadmium adsorption onto orange peel calculated from various methods: a comparison study. Journal of Environmental Chemical Engineering 4, 2671–2682.
Un, U.T., Onpeker, S.E., Ozel, E., 2017. The treatment of chromium containing wastewater using electrocoagulation and the production of ceramic pigments from the resulting sludge. J. Environ. Manag. 200, 196–203.
USGS, 2018. Mineral Community Summaries 2018. U.S. Geological Survey.
Vellingiri, K., Philip, L., Kim, K.-H., 2017. Metal–organic frameworks as media for the catalytic degradation of chemical warfare agents. Coord. Chem. Rev. 353, 159–179.
Vikrant, K., Kim, K.-H., 2019. Nanomaterials for the adsorptive treatment of Hg(II) ions from water. Chem. Eng. J. 358, 264–282.
Vikrant, K., Kim, K.-H., Ok, Y.S., Tsang, D.C., Tsang, Y.F., Giri, B.S., Singh, R.S., 2018. Engineered/designer biochar for the removal of phosphate in water and wastewater. Sci. Total Environ. 616, 1242–1260.
Vikrant, K., Kumar, V., Vellingiri, K., Kim, K.-H., 2019. Nanomaterials for the abatement of cadmium (II) ions from water/wastewater. Nano Res. https://doi.org/10.1007/s12274-019-2309-8.
Vu, V.T., Oh, G.J., Lim, H.P., Yun, K.D., Ryu, S.K., Yim, E.K., Fisher, J.G., Ban, J.S., Park, S.W., 2019. Shear bond strength of zirconia to titanium implant using glass bonding. J. Nanosci. Nanotechnol. 19, 967–969.
Wang, T., Li, Z., 2004. High-temperature reduction of chromium (VI) in solid alkali. J. Hazard. Mater. 112, 63–69.
Wang, H., Yuan, X., Wu, Y., Chen, X., Leng, L., Wang, H., Li, H., Zeng, G., 2015. Facile synthesis of polypyrrole decorated reduced graphene oxide–Fe_3O_4 magnetic composites and its application for the Cr(VI) removal. Chem. Eng. J. 262, 597–606.
Wang, K., Tao, X., Xu, J., Yin, N., 2016a. Novel chitosan–MOF composite adsorbent for the removal of heavy metal ions. Chem. Lett. 45, 1365–1368.
Wang, X., Fan, Q., Chen, Z., Wang, Q., Li, J., Hobiny, A., Alsaedi, A., Wang, X., 2016b. Surface modification of graphene oxides by plasma techniques and their application for environmental pollution cleanup. Chem. Rec. 16, 295–318.
Wang, X., Yu, S., Jin, J., Wang, H., Alharbi, N.S., Alsaedi, A., Hayat, T., Wang, X., 2016c. Application of graphene oxides and graphene oxide-based nanomaterials in radionuclide removal from aqueous solutions. Science Bulletin 61, 1583–1593.
Wang, J., Liang, Y., Jin, Q., Hou, J., Liu, B., Li, X., Chen, W., Hayat, T., Alsaedi, A., Wang, X., 2017a. Simultaneous removal of graphene oxide and Chromium(VI) on the rare earth doped titanium dioxide coated carbon sphere composites. ACS Sustain. Chem. Eng. 5, 5550–5561.
Wang, J., Wang, P., Wang, H., Dong, J., Chen, W., Wang, X., Wang, S., Hayat, T., Alsaedi, A., Wang, X., 2017b. Preparation of molybdenum disulfide coated Mg/Al layered double hydroxide composites for efficient removal of Chromium(VI). ACS Sustain. Chem. Eng. 5, 7165–7174.
Wang, W., Cai, K., Wu, X., Shao, X., Yang, X., 2017c. A novel poly(m-phenylenediamine)/reduced graphene oxide/nickel ferrite magnetic adsorbent with excellent removal ability of dyes and Cr(VI). J. Alloys Compd. 722, 532–543.
Wang, Z., Yang, J., Li, Y., Zhuang, Q., Gu, J., 2017d. Simultaneous degradation and removal of CrVI from aqueous solution with Zr-based metal–organic frameworks bearing inherent reductive sites. Chem Eur J 23, 15415–15423.
Wang, G., Zhang, J., Liu, L., Zhou, J.Z., Liu, Q., Qian, G., Xu, Z.P., Richards, R.M., 2018a. Novel multi-metal containing MnCr catalyst made from manganese slag and chromium wastewater for effective selective catalytic reduction of nitric oxide at low temperature. J. Clean. Prod. 183, 917–924.
Wang, W., Hao, X., Chen, S., Yang, Z., Wang, C., Yan, R., Zhang, X., Liu, H., Shao, Q., Guo, Z., 2018b. pH-responsive Capsaicin@chitosan nanocapsules for antibiofouling in marine applications. Polymer 158, 223–230.
Wang, Y., Chen, Y., Wen, Q., 2018c. Microbial fuel cells: enhancement with a polyaniline/carbon felt capacitive bioanode and reduction of Cr (VI) using the intermittent operation. Environ. Chem. Lett. 16, 319–326.
Wen, T., Wang, J., Yu, S., Chen, Z., Hayat, T., Wang, X., 2017. Magnetic porous carbonaceous material produced from tea waste for efficient removal of As(V), Cr(VI), humic acid, and dyes. ACS Sustain. Chem. Eng. 5, 4371–4380.
Wu, Y., Pang, H., Liu, Y., Wang, X., Yu, S., Fu, D., Chen, J., Wang, X., 2019. Environmental remediation of heavy metal ions by novel-nanomaterials: a review. Environ. Pollut. 246, 608–620.
Xu, W., Zhang, H., Li, G., Wu, Z., 2016. A urine/Cr(VI) fuel cell — electrical power from processing heavy metal and human urine. J. Electroanal. Chem. 764, 38–44.
Xu, C., Yang, W., Liu, W., Sun, H., Jiao, C., Lin, A.-j., 2018. Performance and mechanism of Cr(VI) removal by zero-valent iron loaded onto expanded graphite. J. Environ. Sci. 67, 14–22.
Yang, Z., Hao, X., Chen, S., Ma, Z., Wang, W., Wang, C., Yue, L., Sun, H., Shao, Q., Murugadoss, V., Guo, Z., 2019. Long-term antibacterial stable reduced graphene oxide nanocomposites loaded with cuprous oxide nanoparticles. J. Colloid Interface Sci. 533, 13–23.
Yao, W., Ni, T., Chen, S., Li, H., Lu, Y., 2014. Graphene/Fe_3O_4@polypyrrole nanocomposites as a synergistic adsorbent for Cr(VI) ion removal. Compos. Sci. Technol. 99, 15–22.
Zare, E.N., Motahari, A., Sillanpää, M., 2018. Nanoadsorbents based on conducting polymer nanocomposites with main focus on polyaniline and its derivatives for removal of heavy metal ions/dyes: a review. Environ. Res. 162, 173–195.

Zhang, H., Xu, W., Wu, Z., Zhou, M., Jin, T., 2013. Removal of Cr(VI) with cogeneration of electricity by an alkaline fuel cell reactor. J. Phys. Chem. C 117, 14479–14484.
Zhang, S., Wang, X., Li, J., Wen, T., Xu, J., Wang, X., 2014. Efficient removal of a typical dye and Cr(vi) reduction using N-doped magnetic porous carbon. RSC Adv. 4, 63110–63117.
Zhang, Q., Yu, J., Cai, J., Zhang, L., Cui, Y., Yang, Y., Chen, B., Qian, G., 2015. A porous Zr-cluster-based cationic metal–organic framework for highly efficient $Cr_2O_7^{2-}$ removal from water. Chem. Commun. 51, 14732–14734.
Zhang, L., Yu, W., Han, C., Guo, J., Zhang, Q., Xie, H., Shao, Q., Sun, Z., Guo, Z., 2017. Large scaled synthesis of heterostructured electrospun TiO_2/SnO_2 nanofibers with an enhanced photocatalytic activity. J. Electrochem. Soc. 164, H651–H656.
Zhang, K., Li, H., Xu, X., Yu, H., 2018a. Synthesis of reduced graphene oxide/NiO nanocomposites for the removal of Cr(VI) from aqueous water by adsorption. Microporous Mesoporous Mater. 255, 7–14.
Zhang, P., Ge, T., Yang, H., Lin, S., Cao, Y., Zhao, C.X., Liu, H., Umar, A., Guo, Z., 2018b. Antifouling of titania nanostructures in real maritime conditions. Sci. Adv. Mater. 10, 1216–1223.
Zhang, S.-H., Wu, M.-F., Tang, T.-T., Xing, Q.-J., Peng, C.-Q., Li, F., Liu, H., Luo, X.-B., Zou, J.-P., Min, X.-B., 2018c. Mechanism investigation of anoxic Cr (VI) removal by nano zero-valent iron based on XPS analysis in time scale. Chem. Eng. J. 335, 945–953.
Zhang, X., Wang, X., Liu, X., Lv, C., Wang, Y., Zheng, G., Liu, H., Liu, C., Guo, Z., Shen, C., 2018e. Porous polyethylene bundles with enhanced hydrophobicity and pumping oil-recovery ability via skin-peeling. ACS Sustain. Chem. Eng. 6, 12580–12585.
Zhang, H., Lyu, S., Zhou, X., Gu, H., Ma, C., Wang, C., Ding, T., Shao, Q., Liu, H., Guo, Z., 2019. Super light 3D hierarchical nanocellulose aerogel foam with superior oil adsorption. J. Colloid Interface Sci. 536, 245–251.
Zhao, B., Shao, Q., Hao, L., Zhang, L., Liu, Z., Zhang, B., Ge, S., Guo, Z., 2018a. Yeast-template synthesized Fe-doped cerium oxide hollow microspheres for visible photodegradation of acid orange 7. J. Colloid Interface Sci. 511, 39–47.
Zhao, J., Ge, S., Liu, L., Shao, Q., Mai, X., Zhao, C.X., Hao, L., Wu, T., Yu, Z., Guo, Z., 2018b. Microwave solvothermal fabrication of zirconia hollow microspheres with different morphologies using pollen templates and their dye adsorption removal. Ind. Eng. Chem. Res. 57, 231–241.
Zhao, J., Ge, S., Pan, D., Shao, Q., Lin, J., Wang, Z., Hu, Z., Wu, T., Guo, Z., 2018c. Solvothermal synthesis, characterization and photocatalytic property of zirconium dioxide doped titanium dioxide spinous hollow microspheres with sunflower pollen as bio-templates. J. Colloid Interface Sci. 529, 111–121.
Zhao, J., Ge, S., Pan, D., Pan, Y., Murugadoss, V., Li, R., Xie, W., Lu, Y., Wu, T., Wujcik, E.K., Shao, Q., Mai, X., Guo, Z., 2019. Microwave hydrothermal synthesis of In_2O_3-ZnO nanocomposites and their enhanced photoelectrochemical properties. J. Electrochem. Soc. 166, H3074–H3083.
Zhou, X., Lv, B., Zhou, Z., Li, W., Jing, G., 2015. Evaluation of highly active nanoscale zero-valent iron coupled with ultrasound for chromium(VI) removal. Chem. Eng. J. 281, 155–163.
Zhou, J., Wang, Y., Wang, J., Qiao, W., Long, D., Ling, L., 2016. Effective removal of hexavalent chromium from aqueous solutions by adsorption on mesoporous carbon microspheres. J. Colloid Interface Sci. 462, 200–207.
Zhu, F., Ma, S., Liu, T., Deng, X., 2018. Green synthesis of nano zero-valent iron/Cu by green tea to remove hexavalent chromium from groundwater. J. Clean. Prod. 174, 184–190.